Lawrence Berkeley National Laboratory
Recent Work

Title
YIELDING AND PLASTIC FLOW OF POLYCRYSTAINLINE NIOBIUM

Permalink
https://escholarship.org/uc/item/6nt9z0gm

Author
Torne, Lenon Ivan. Van

Publication Date
1962-08-01

eScholarship.org Powered by the California Digital Library
University of California

UCRL-10356

University of California

Ernest O. Lawrence Radiation Laboratory

TWO-WEEK LOAN COPY

This is a Library Circulating Copy which may be borrowed for two weeks. For a personal retention copy, call Tech. Info. Division, Ext. 5545

YIELDING AND PLASTIC FLOW OF POLYCRYSTALLINE NIOBIUM

Berkeley, California

DISCLAIMER

This document was prepared as an account of work sponsored by the United States Government. While this document is believed to contain correct information, neither the United States Government nor any agency thereof, nor the Regents of the University of California, nor any of their employees, makes any warranty, express or implied, or assumes any legal responsibility for the accuracy, completeness, or usefulness of any information, apparatus, product, or process disclosed, or represents that its use would not infringe privately owned rights. Reference herein to any specific commercial product, process, or service by its trade name, trademark, manufacturer, or otherwise, does not necessarily constitute or imply its endorsement, recommendation, or favoring by the United States Government or any agency thereof, or the Regents of the University of California. The views and opinions of authors expressed herein do not necessarily state or reflect those of the United States Government or any agency thereof or the Regents of the University of California.

Research and Development

UCRL-10356
UC-25 Metals,
Ceramics, and Materials
TID-4500 (17th Ed.)

UNIVERSITY OF CALIFORNIA
Lawrence Radiation Laboratory
Berkeley, California

Contract No. W-7405-eng-48

YIELDING AND PLASTIC FLOW OF POLYCRYSTALLINE NIOBIUM

Lenon Ivan Van Torne
Masters Thesis
August 1962

Reproduced by the
Technical Information Division
directly from author's copy

Printed in USA. Price $1.50. Available from the
Office of Technical Services
U. S. Department of Commerce
Washington 25, D.C.

Table of Contents

Table of Contents (continued)

ABSTRACT

Transmission electron microscopy techniques were used to study the process of yielding and plastic flow in polycrystalline Nb by observing the dislocation substructure resulting from tensile deformation.

The tensile properties were found to vary markedly with the amount and distribution of impurity solute atoms. The amount and distribution of impurities varied with the annealing conditions. Annealing at 1000°C resulted in the formation of networks of precipitate plates in addition to solute atom clusters. Annealing at higher temperatures, 1700-2100°C, resulted in a distribution of solute atom clusters 50 to 150Å in diameter.

The lower yield shear stress was found to be given by the expression:

$$\tau_{ly} = \tau_f + \tau_{structure}$$

where τ_f = a friction stress determined from dislocation radii measurements, and could be factored into two terms, τ_o and $\tau_{soln.}$

τ_o = a lattice friction stress and was found to be about $0.8 \left(\frac{kg}{mm^2}\right)$

$\tau_{soln.}$ = contribution to τ_f from solute atoms atomistically in solution

$\tau_{structure} = G\epsilon^2 C$

G = shear modulus

ϵ = solute atom lattice dilation parameter

C = atom fraction of metallic plus interstitial impurities.

Specimens containing precipitate networks formed a well defined dislocation cell structure when deformed in tension. The flow stress-dislocation density relations in these specimens was found to be

$$\sigma_{fl}\ (\frac{kg}{cm^2}) = 0.85Gb\rho^{\frac{1}{2}} + \text{constant.}$$

Specimens containing no precipitate networks did not develop a dislocation cell structure when deformed in tension. The flow stress-dislocation density relation in these specimens was found to be

$$\sigma_{fl}\ (\frac{kg}{cm^2}) = 6.5 \times 10^{3}Gb\rho^{\frac{1}{7}} + \text{constant.}$$

INTRODUCTION

Until recently the use of transmission electron microscopy to study dislocation substructures and interactions in the refractory metals miobium, molybdenum, tantalum and tungsten has been only slightly utilized. Benson, Thomas and Washburn[1] have studied dislocation substructures in Mo due to deformation and annealing. Nakayama, Weissmann and Imura[2] have studied the annealing substructure in W in which they observed stacking faults which were attributed to impurity segregation. Weissmann[2] has studied the deformation structure of Ta, and some work has been done on Nb[2, 3]. In the early work stacking faults in Nb had been reported, but with the attainment of more pure Nb observations of stacking faults were no longer observed.

Although some observations of the dislocation substructure of fatigued Nb have been made[2], a thorough investigation of the substructure resulting from tensile deformation has not been carried out. Such an investigation has been undertaken here, wherein grain size and impurity effects on yielding and plastic flow were studied. The objective of the research was to gain a better understanding of the mechanism of yielding which for BCC metals is usually expressed by the empyrical Petch[4] equation:

$$\tau_{yield} = \tau_{friction} + \frac{K}{d^{\frac{1}{2}}}$$

where τ = yield stress

$\tau_{friction}$ = friction stress

K = a parameter which applies to the given BCC metal

d = the average grain diameter,

and to correlate the dislocation substructure with the mechanical

properties. In this way it is also possible to gain further knowledge about the process of plastic flow.

3 Experimental Procedure

3.1 Material Analysis

The Nb sheet used in this investigation was of the highest purity commercially available at that time. The chemical analysis of the as received Nb is given in Table 1.

Table 1

element	Group I	Group II
Al	<0.002	0.0165
C	0.002	<0.0020
Fe	0.010	0.0292
N_2	0.007	0.0288
O_2	0.018	<0.0020
Si	<0.010	0.0150
Ta	0.061	
Ti	<0.015	0.0060
H_2	0.001	

Nb Chemical Analysis in Weight Percent*

* The interstitial content varies with the annealing treatment.

The specimens were reduced about ten percent by cold rolling prior to annealing. Annealing of the specimens in a vacuum of 10^{-6} to 10^{-5}mm Hg was employed to remove the interstitials such as carbon, nitrogen, oxygen and hydrogen. The quality of the vacuum system employed was sufficient to reduce the interstitial concentration to very low values but the leak rate of a system, given in micronliters

per hour, is directly proportional to the volume of the vacuum system. Since the volume of the original system used was 100 liters the leak rate was such that only marginal results were obtained in removing interstitials. The best purity attained with this large system was a total interstitial atom fraction equal to 1.47×10^{-3}. At a later date interstitial purities better than 0.25×10^{-3} atom fraction were obtained using induction heating and a vacuum system volume of 1 liter.

The analysis of the gases namely nitrogen, oxygen and hydrogen was made by a vacuum fusion technique. The carbon content was determined by employing a conductometric method.

3.2 Specimen Preparation

The material was cut into tensile specimens three inches long by one half inch wide. The thickness of the sheet stock was 0.005 inches. The specimens were then annealed in the vacuum furnace shown in Fig. 1. The annealing temperatures and times employed were those yielding the best quality vacuum. The temperatures used did not exceed 2100°C and the time at temperature was never less than two hours. At the end of the anneal the furnace was cooled slowly, the time to come to ambient temperature being about two hours. By varying the annealing temperature it was possible to vary the impurity content of the initial Nb. This also resulted in different grain sizes.

Prior to tensile testing, the specimens were chemically polished in a solution of 40% hydrofluoric acid and 60% concentrated nitric acid to obtain a smooth specimen surface and to remove any sharp edges that may have been present.

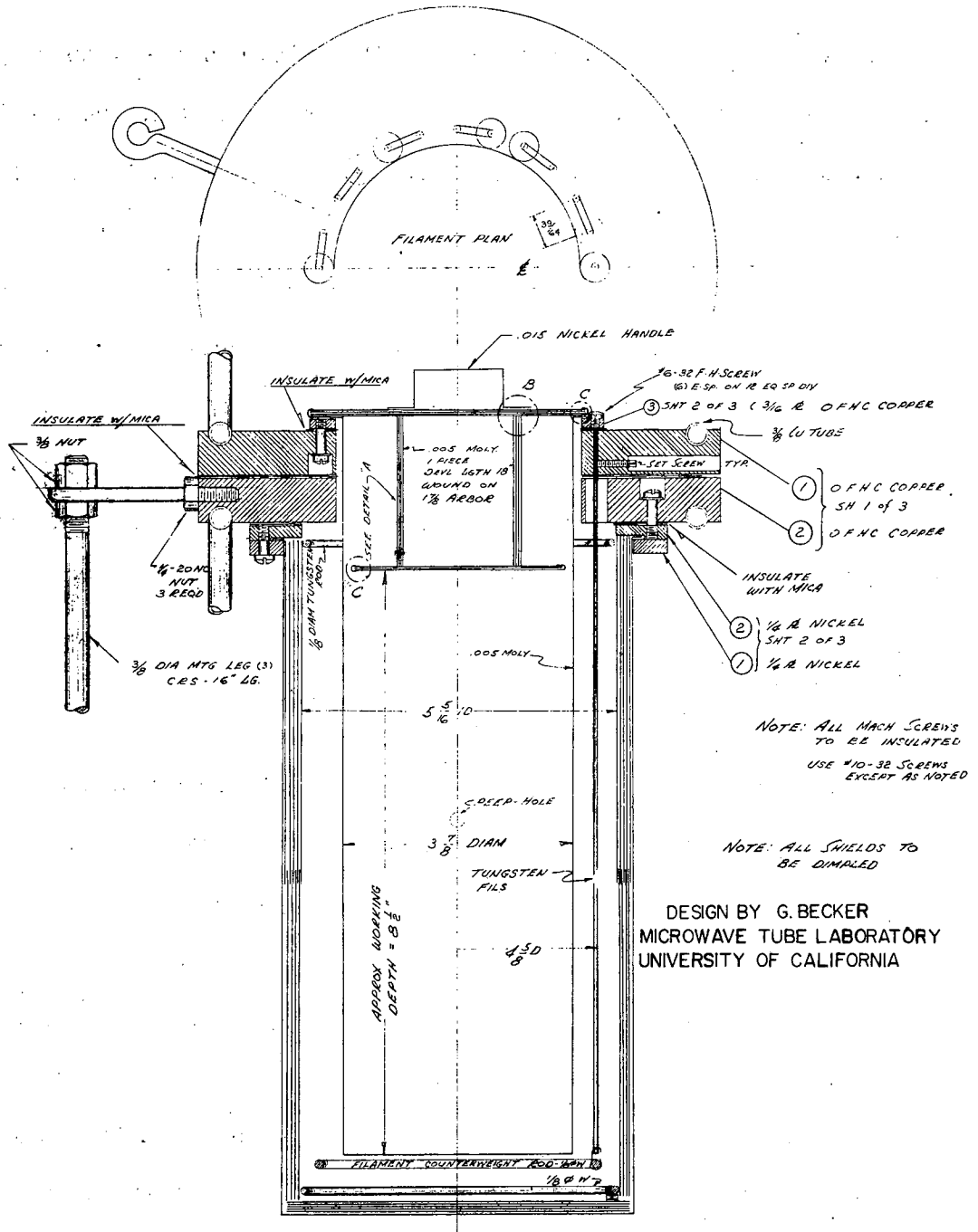

NOTE: ALL MACH SCREWS TO BE INSULATED
USE #10-32 SCREWS EXCEPT AS NOTED

NOTE: ALL SHIELDS TO BE DIMPLED

DESIGN BY G. BECKER
MICROWAVE TUBE LABORATORY
UNIVERSITY OF CALIFORNIA

FIGURE I. VACUUM ANNEALING FURNACE

MUB-1200

An Instron Universal testing machine was used for the tensile deformation. The full scale load deflection employed was 100 pounds. All the specimens were strained at a rate equal to 3.33×10^{-4} per sec. over a gauge length of one inch.

Thin foils, about 3000Å thick, suitable for transmission electron microscopic examination were prepared after tensile deformation, using the "window technique" of chemical polishing[5]. The masking material for the window was a solution of polystyrene dissolved in benzene. This solution was reasonably inert to the HF in the chemical polish. The polishing solution was prepared from 40 vol. percent concentrated hydrofluoric acid and 60 vol. percent concentrated nitric acid. The temperature of the polishing solution was maintained just above 0°C by means of an ice bath. Satisfactory foils were obtained with this technique in about 30 minutes.

3.3 Specimen Examination

The foils were examined in a Siemens Elmiskop Ib electron microscope. An electron accelerating voltage of 100kv and a projector pole piece of 0.77 mm diameter were employed. The resolution possible under these conditions was found to be 9.8Å. Foil orientations were determined by the selected area diffraction technique.

3.3.1 Grain Size

The grain size was determined by using a line intercept technique on not less than five different areas of the specimen. These areas were then photographed with a light microscope. The grain diameter was determined by the ratio of a given length of line divided by the number of

grains intercepted by the line. The grain size reported was taken as the arithmetical average of the five different areas of the specimen.

3.3.2 Dislocation Density

The dislocation densities were determined by a technique described by Ham[6]. It can be shown[7], assuming that the dislocation segments are randomly oriented with respect to the plane of the micrograph, that the dislocation density is given by:

$$\rho = \left(\frac{4}{\pi}\right) \frac{Rp}{At} \quad (\text{lines/cm}^2)$$

where Rp = the projected length of dislocation
A = area of field of view
t = thickness of the foil
$\left(\frac{4}{\pi}\right)$ = a statistical randomness factor

There is much labor involved in the measurement of Rp. However, Rp can be closely estimated by using some results of Smith and Guttman[8]. If a set of random lines is used over A, and the number of dislocation intersections made with the lines is measured, then Rp is given by:

$$Rp = \frac{\pi}{2} \frac{NA}{L}$$

thus $$\rho = \frac{2N}{Lt} \quad (\text{valid for } N>50)$$

where N = number of dislocation intersections with the random lines

L = total length of random line.

The value used for the foil thickness, t, was determined from an analysis of a slip trace, using simple trigonometric relations. The value of t so determined was about 3000Å. Since slip traces were very rarely observed, i.e., only near the cut edge of the foil, it was not

possible to determine the exact thickness for each of the many micrographs used for dislocation density determination.

The electron beam intensity in regions of the foils where dislocation density micrographs were taken was nearly equal to the intensity observed where t was determined from the slip trace. The tilting mechanism on the microscope was fully utilized to obtain the best contrast and maximum intensity in all foils. Hence, only negligible error was introduced in using t equal to 3000Å for all the micrographs.

Micrographs for density measurements were taken from five foils, each of which were taken from five different regions of the specimen gauge length. The area sampled by each micrograph is 3.5 x 4.5 microns equaling 15.75 square microns. The dislocation density was observed to be less near the edge of the foils, therefore all micrographs were taken as far from the foil edge as possible. An example of micrographs used for density measurements are shown in Fig. 2.

3.3.3 Stress Center Wavelength λ

The yield strength of a crystal containing a dispersion of internal stress centers is influenced by the scale of dispersion[9]. In a crystal these stress centers can be any obstacles, such as precipitate particles or clusters of solute atoms or vacancies, which hinder dislocation motion. An example of the measurement of the distance between stress centers λ, i.e., the wavelength of a pinned dislocation is shown in Fig. 3.

3.3.4 Friction Stress

An indication of the effect of friction on dislocation motion

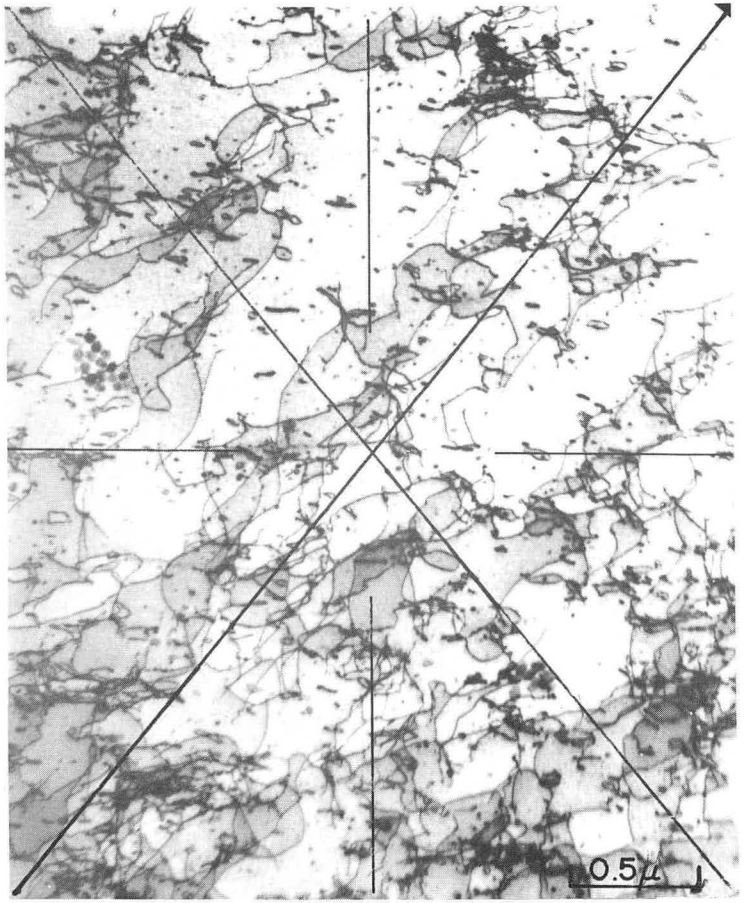

σ_{fl} = 17.3 kg/mm^2 , ϵ_p = 4.4%

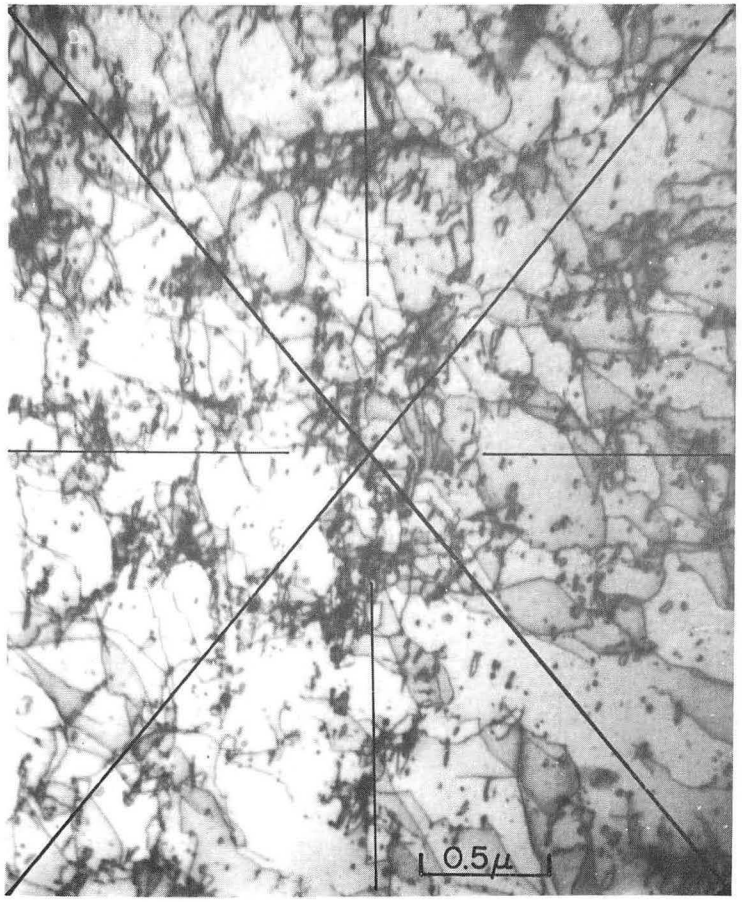

σ_{fl} = 19.0 kg/mm^2, ϵ_p = 7.4%

FIGURE 2. EXAMPLES OF DISLOCATION DENSITY MEASUREMENTS.

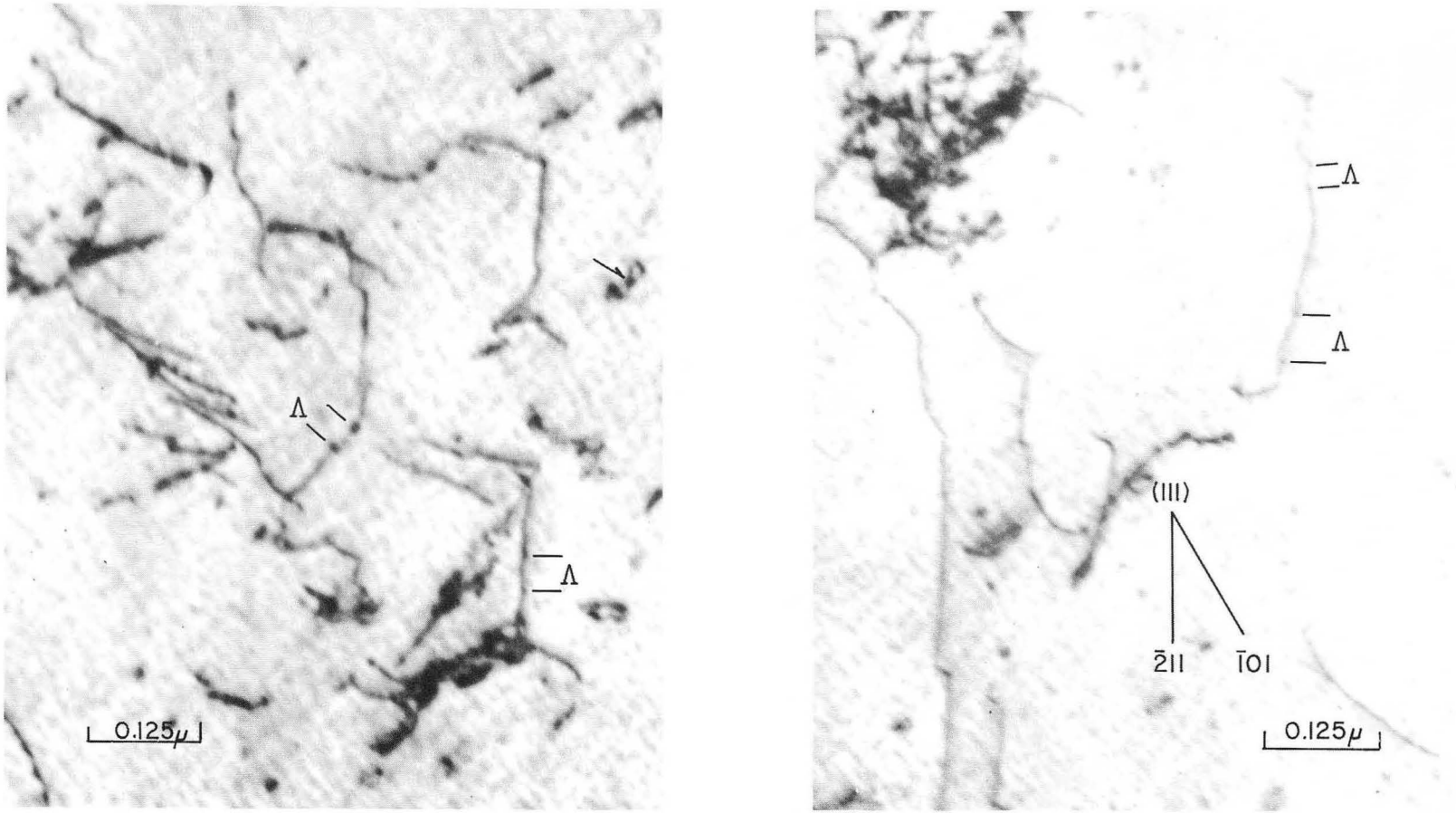

FIGURE 3. EXAMPLES OF Λ MEASUREMENTS.

imposed by the crystal structure and solute atoms in solution can be obtained from observations of the radius of curvature of isolated dislocations. If it is assumed that in the absence of jogs or any applied stress the dislocation curvature is due to equilibrium between the line tension and the friction stress of the crystal, then the friction stress can be calculated from the measured radius of curvature. Examples of how this radius of curvature was measured are shown in Fig. 4. It is quite clear that many radii orientations are possible. However, due to geometrical limitations, only dislocations that lie in planes nearly parallel to the plane of the foil could be measured. In order to make the assumptions more valid, only smoothly curving dislocations far from resolvable sources of internal stress were measured.

4 Experimental Results

4.1 Tensile Stress-Strain Curves

Niobium, like other body centered cubic metals, exhibits a semidiscontinuous stress-strain curve. The interesting points on the tensile stress-strain curve are, the elastic limit, the upper and lower yield points and the flow stress, as shown in Fig. 5. A series of tensile stress-strain curves selected from more than 50 tests of polycrystalline Nb of various purity levels are shown in Fig. 6. It is immediately evident that the level of impurity has a marked influence on the stress-strain curve. The purity for each curve is given in Table 2.

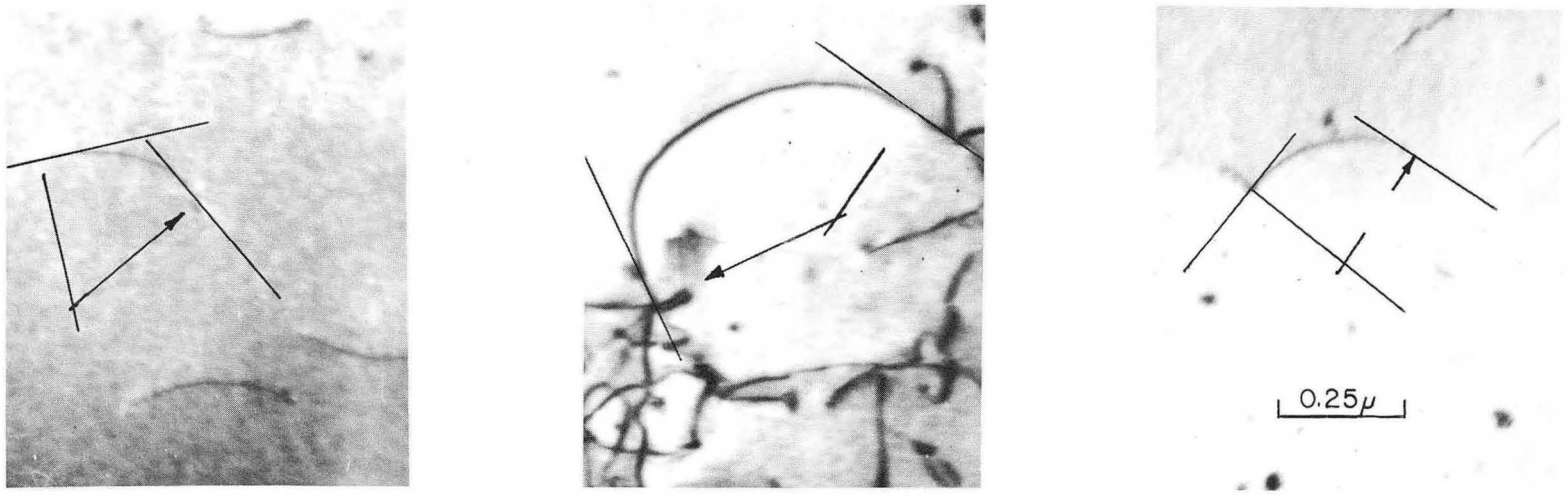

FIGURE 4. EXAMPLES OF DISLOCATION RADIUS MEASUREMENTS.

ZN-3225

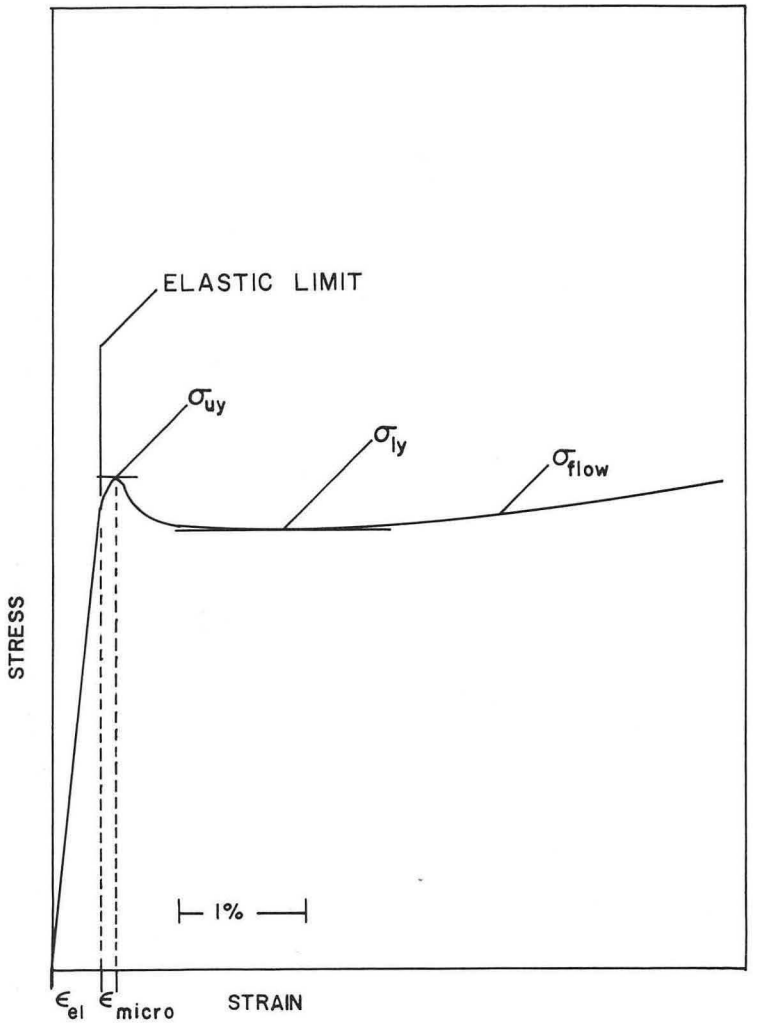

FIGURE 5. IDEAL Nb STRESS - STRAIN CURVE

MU-27849

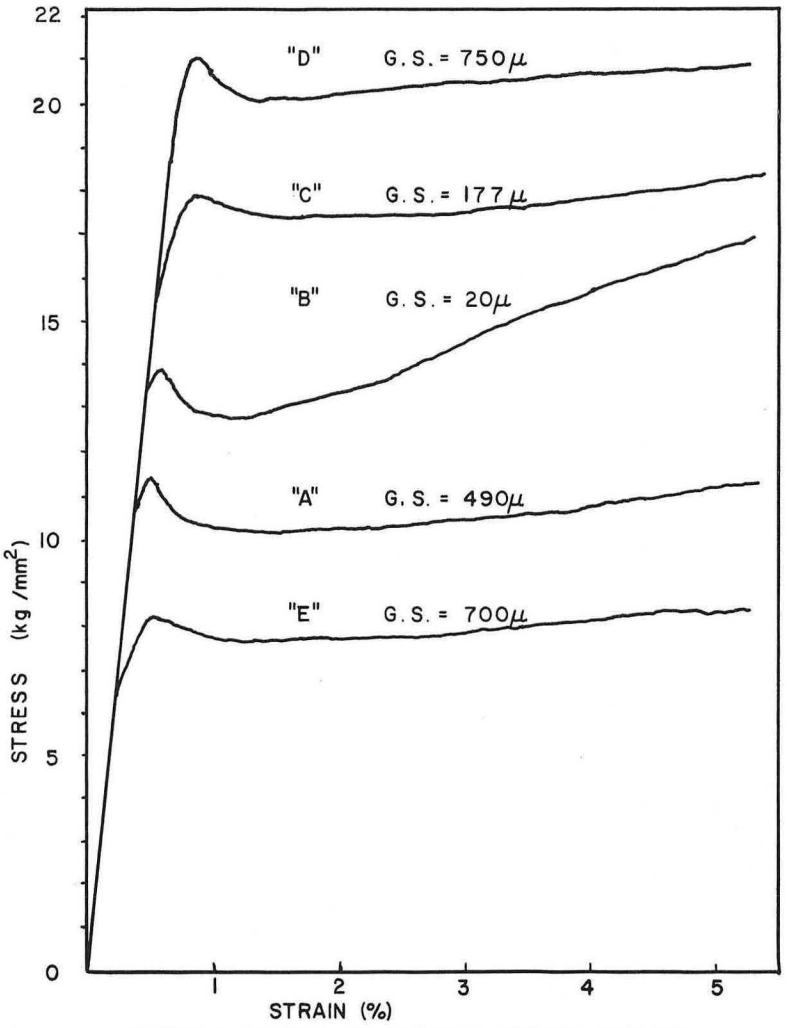

FIGURE 6. TYPICAL Nb STRESS-STRAIN CURVES.

MU-27850

Table 2

Tensile Curve	Atom Fraction of Impurity (metallic + interstitial)
"A"	2.60×10^{-3}
"B"	3.80×10^{-3}
"C"	5.30×10^{-3}
"D"	6.50×10^{-3}
"E"	1.50×10^{-3}

Impurity levels corresponding to tensile curves of Fig. 6.

The effect of increasing the impurity content is to shift the portion of the curve in the plastic strain range to higher stress levels.

Tensile curve "B" in Fig. 6 is conspicuous since this curve has a greater increase in flow stress for a given increment in strain when compared to the other curves. Tensile curve "B" represents a group of specimens that were received in the as annealed condition. The annealing treatment reported for this group was 1000°C for two hours in a vacuum pressure of less than 10^{-5} mm Hg. Since the yield strength corresponds to Nb in the annealed condition for the given impurity level, the annealing cycle was accepted as reported. All the other specimens which are represented by the tensile curves "A", "C", "D" and "E" were annealed as was discussed in the experimental procedure.

There was a very striking difference in the dislocation substructure of the specimens corresponding to tensile curve "B" as compared to the dislocation substructure of the specimens which gave the other tensile curves. In "B" specimens there exist precipitate plates grown from network dislocations as shown in Fig. 7. This type of substructure is common to all the specimens giving curves of type "B", however, it was not

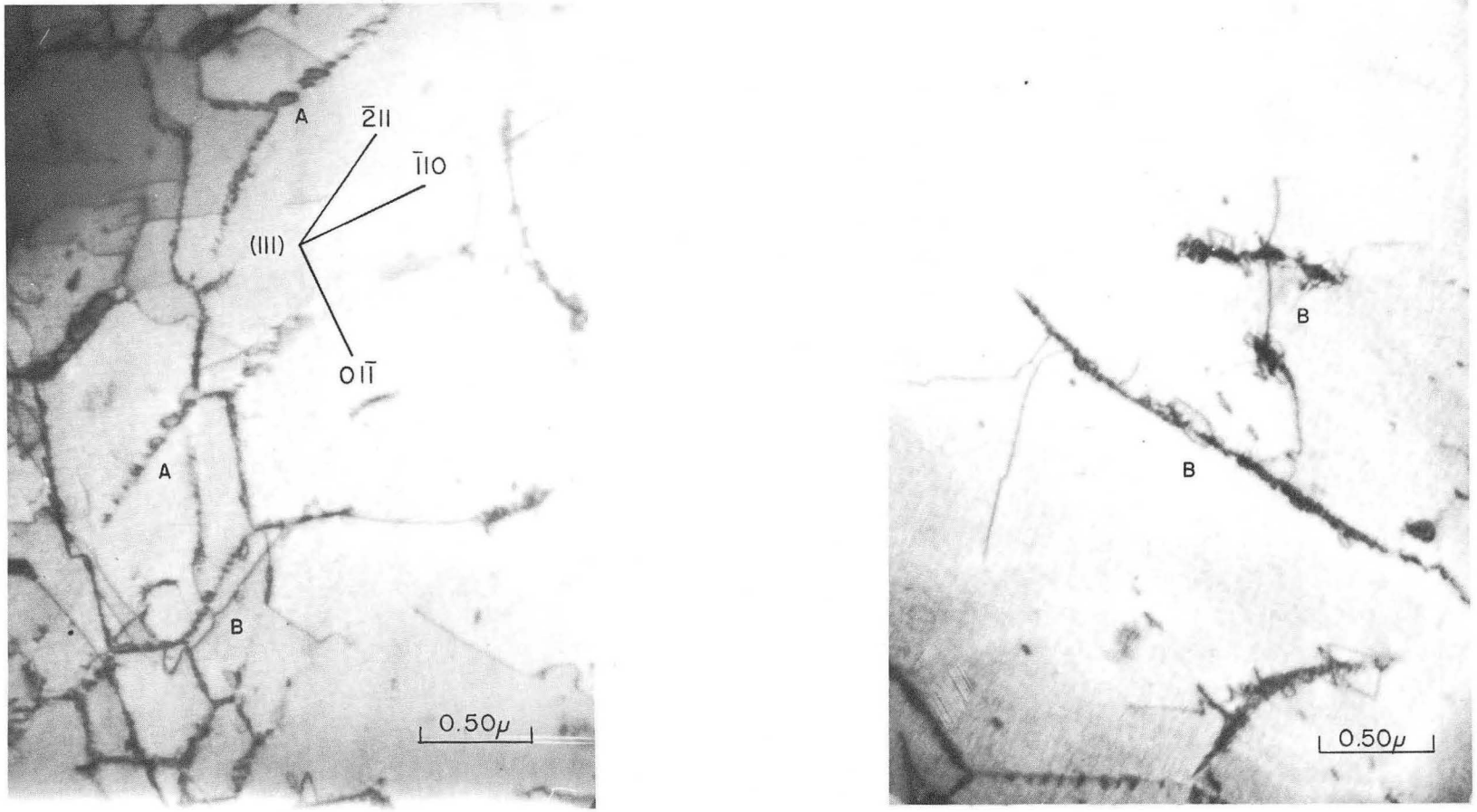

FIGURE 7. PRECIPITATE PLATES ON NETWORK DISLOCATIONS.

ZN-3226

observed in the other specimens. The implications of this type of substructure will be discussed in a later section (5.4).

It is generally accepted that the plastic deformation of BCC metals is concomitant with the initiation of a Luders band at points of stress concentration within the specimen. Deformation then proceeds by the growth and lengthening of the band as it moves across the specimen. Nb plastically deforms in a similar manner. Luders bands have been observed on the surfaces of deformed specimens. The surface of a deformed specimen is shown in Fig. 8. These bands originated at the junction of the specimen and the tensile grips. As the specimen deforms the bands propagate across the specimen at an angle of about 45° to the tensile axis. The band front progresses from the tensile grips toward the center of the gauge length. The observed behavior is hardly surprising since the junction between the specimen and the grips is a region of stress concentration, and further, the maximum shear stress occurs at an angle of 45° to the tensile axis.

The cross sectional area of the specimens limited the amount of plastic deformation obtainable, before failure, to about 20 percent. Deformation approaching this strain level produced a roughening of the originally smooth surface of the specimen, as shown at the top of Fig. 8. This effect is due to grain rotation whereby the normal to the slip plane and the slip direction tend to become coincident with the tensile axis.

4.1.1 Elastic Limit

The elastic limit is considered here to be the point on the initial portion of the stress-strain curve where the curve is first detected

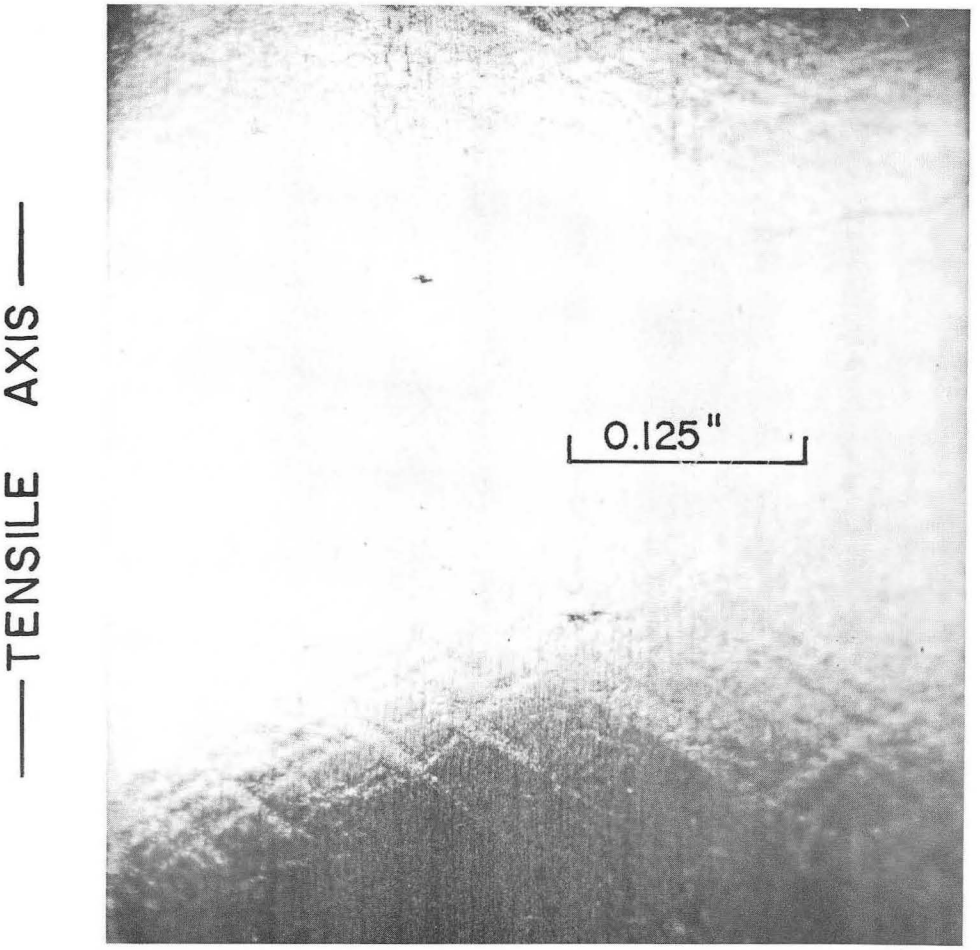

FIGURE 8. LÜDER BANDS ON Nb SPECIMEN SURFACE.

ZN-3227

to deviate from a straight line, as shown in Fig. 5. However, this point is dependent upon the precision with which the strain can be measured in addition to the strain rate. In this investigation the precision of strain measurement employed was 0.02 percent. The elastic limit appears, under the test conditions used, to correspond approximately to a stress level equal to the lower yield stress.

4.1.2 Upper Yield Point

Upper yield points were observed for all the Nb specimens. If the specimen was unloaded after the upper yield point had appeared and then immediately reloaded, no upper yield point was observed upon subsequent reloading.

The average magnitude of yield drop given by:

$$\tau_{uy} - \tau_{ly}$$

where τ_{uy} = the upper yield shear stress

τ_{ly} = the lower yield shear stress

$\tau_{uy} = \frac{\sigma_{uy}}{2}$, i.e., a von Mises approximation

$\tau_{ly} = \frac{\sigma_{ly}}{2}$

was observed to be $0.40(\frac{kg}{mm^2})$. Here the greek letter τ will be used to signify shear stress, the greek letter σ will be used to signify tensile stress, and ϵ will be used for strain.

4.1.3 Lower Yield Point

The lower yield stress is a more reproducible measure of the strength of the specimen since τ_{ly} is not as sensitive to specimen alignment in the tensile machine as τ_{uy}. Therefore the lower yield stress

was considered to be a better measure of the strength of the specimen.

When τ_{ly} is plotted versus the atom fraction of metallic plus interstitial impurities (O, N, C, and H) a straight line of positive slope results as shown in Fig. 9. The range of τ_{ly} observed is shown together with the average of the range. A least squares fit of the average points yields:

$$\tau_{ly} \left(\frac{kg}{mm^2}\right) = 1.75 + 1.26 \times 10^3 \times (\text{Atomic Fraction})$$

A linear relation between τ_{ly} and percent oxygen has been observed in Nb by Leadbetter and Argent[10].

Mott and Nabarro[9] have considered the effect of internal stress centers such as isolated and clustered solute atoms on the yield strength of crystals. When the wavelength of the stress centers is much less than the limiting radius of curvature of a dislocation, i.e.,

$$\lambda < \frac{Gb}{2\tau_{yield}} .$$

Nabarro has shown that the yield strength of a polycrystalline specimen is approximately:

$$\tau = G\epsilon^2 C.$$

Here G = shear modulus, for Nb, $G = 3.82 \times 10^3 \left(\frac{kg}{mm^2}\right)$ [11]

b = burgers vector, for Nb, $b = 2.86\text{Å}$

ϵ = an atomic misfit parameter defined by:

$$\epsilon = \frac{(r_{solute} - r_{solvent})}{r_{solvent}}$$

r_{solute} = radius of the solute atom

$r_{solvent}$ = radius of the solvent atom

c = concentration of solute as the atomic fraction.

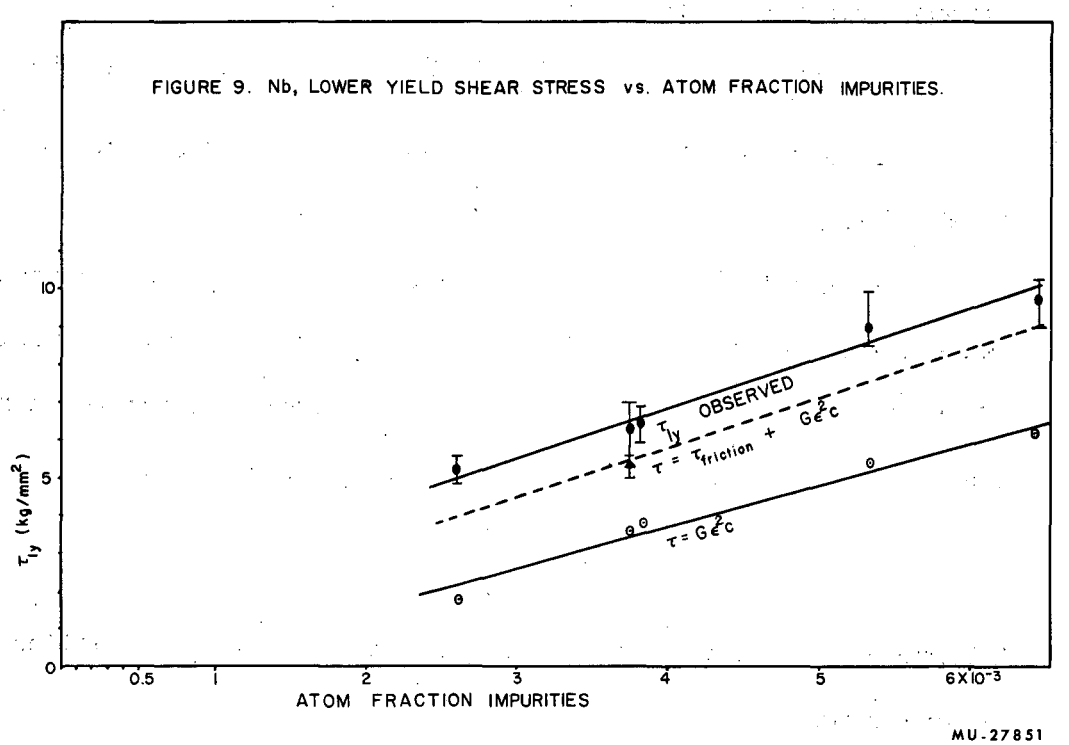

FIGURE 9. Nb, LOWER YIELD SHEAR STRESS vs. ATOM FRACTION IMPURITIES.

The values of r_{solute} used for the calculation of ϵ are shown in Table 3.

Table 3

Element	Atomic "Radius" (Å)	Ref.	$\epsilon = \frac{(r_{solute} - r_{solvent})}{r_{solvent}}$
Nb	1.429	(12)	o
Ta	1.430	"	0.670×10^{-3}
Ti(BCC)	1.45	"	1.47×10^{-2}
Si(DC)	1.18	"	-1.74×10^{-1}
Fe(BCC)	1.24	"	-1.32×10^{-1}
Al	1.43	"	0.670×10^{-3}
C	0.74	(13)	-4.82×10^{-1}
N	0.73	"	-4.89×10^{-1}
O	0.73	"	-4.89×10^{-1}
H	0.35	"	-0.755

Values of r_{solute} for impurities and ϵ

When τ calculated from the above expression is plotted versus atomic fraction of impurity the lower line in Fig. 9. is obtained. A linear least squares fit of a line to these points yields,

$$\tau \left(\frac{kg}{mm^2}\right) = 1.09 \times 10^3 \left(\frac{kg}{mm^2}\right) \times C \text{ (Atomic Fraction)} - 0.705.$$

It is evident from the slope of this line that a theoretical model based on interactions of dislocation strain fields with the dilational strain fields of solute atoms and or clusters predicts a dependence of yield strength similar to what is observed.

4.1.4 Friction Stress

The calculated values of τ_f from measured radii of isolated curved dislocations are plotted versus atom fraction of impurities in Fig. 10. The mean and τ_f plus and minus a standard deviation are shown. Each range represents not less than 19 measurements, nor more than 46. A probability plot of each range is shown in Fig. 11, 12, 13 and 14. A least squares line for the mean points gives:

$$\tau_f \ (\tfrac{kg}{mm^2}) = 0.805 + 0.279 \times 10^{3} \times (\text{Atom Fraction}).$$

The resulting line shows that τ_f probably has some dependence on the impurity content of the crystal.

4.1.5 Flow Stress versus Plastic Strain

The functional relation between the flow stress σ_{fl} and plastic strain was determined for the two types of experimental tensile stress-strain curves. The values of σ_{fl} and ϵ_p were taken from the tensile curve "B". The log σ_{fl} versus log ϵ_p was then plotted as shown in Fig. 15(a). The slope of this curve was then determined, yielding:

$$\log \sigma_{fl} = 0.25 \log \epsilon_p + \log \text{constant}.$$

In exponential form the relation is:

$$\sigma_{fl} = \epsilon_p^{\frac{1}{4}} + \text{constant}.$$

To determine the functional relationship between σ_{fl} and ϵ_p for the tensile curves of type "A", "C", "D" and "E", which are obviously different than type "B", the same method was used. The log σ_{fl} versus log ϵ_p are shown in Fig. 15(b). The slope of this curve gave:

$$\log \sigma_{fl} = \frac{17}{169} \log \epsilon_p + \log \text{constant}.$$

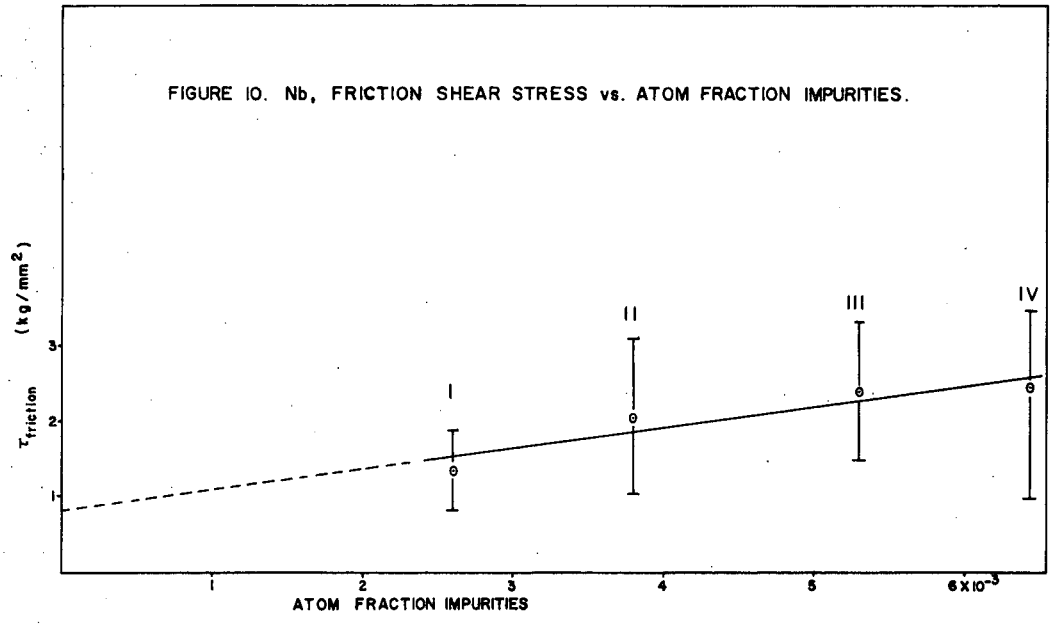
FIGURE 10. Nb, FRICTION SHEAR STRESS vs. ATOM FRACTION IMPURITIES.
$\tau_{friction}$ (kg/mm^2)
3
2
1
I
II
III
IV
1
2
3
4
5
6X10^{-3}
ATOM FRACTION IMPURITIES
MU-27852

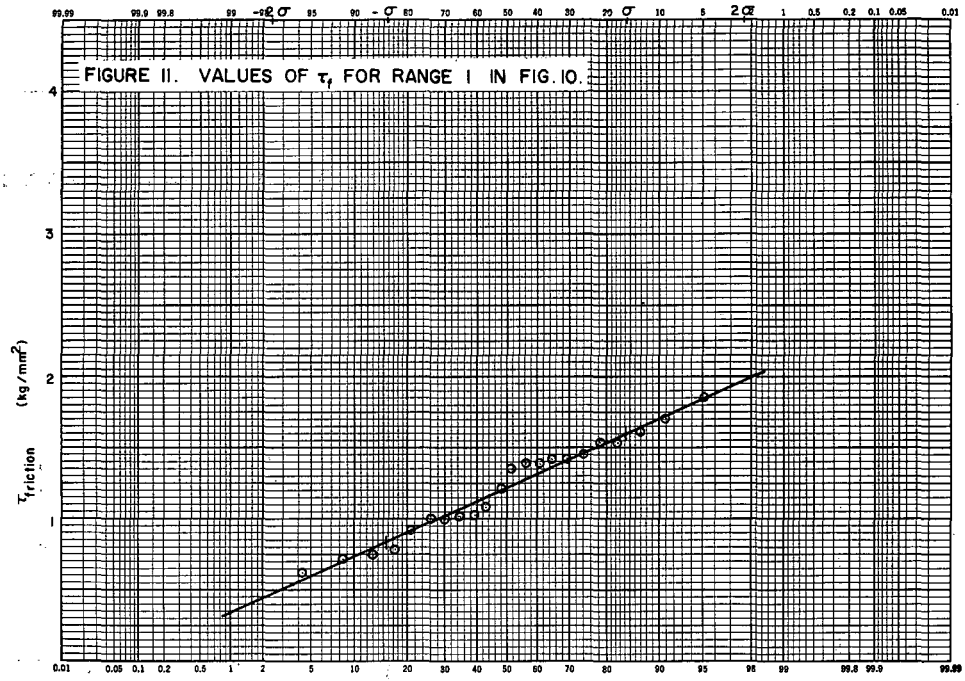

FIGURE II. VALUES OF τ_f FOR RANGE I IN FIG. IO.

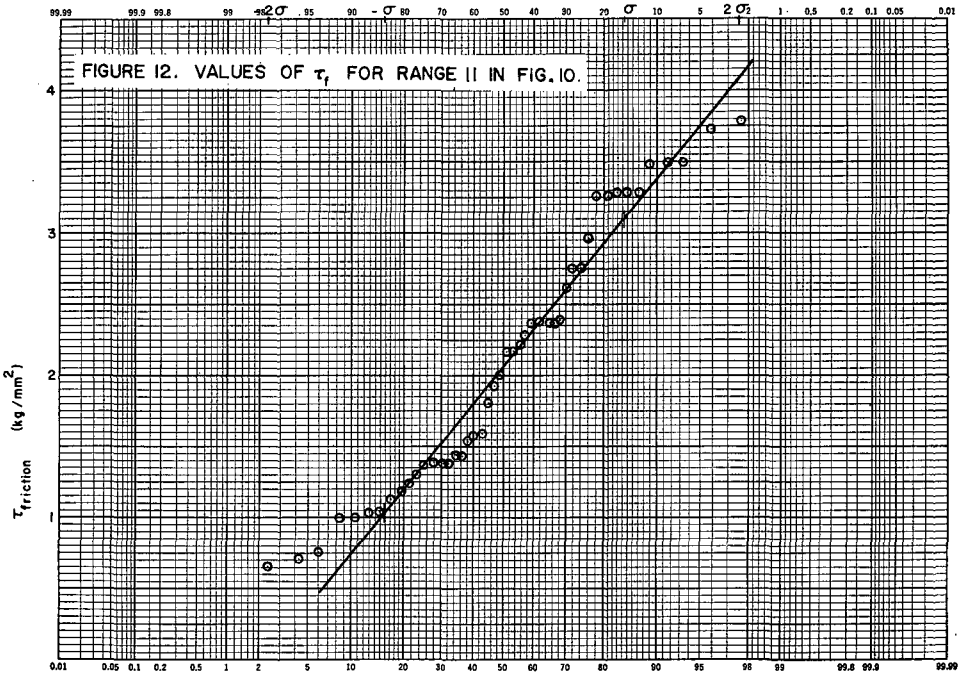
FIGURE 12. VALUES OF τ_f FOR RANGE II IN FIG. 10.
$\tau_{friction}$ (kg/mm^2)
MU-27854

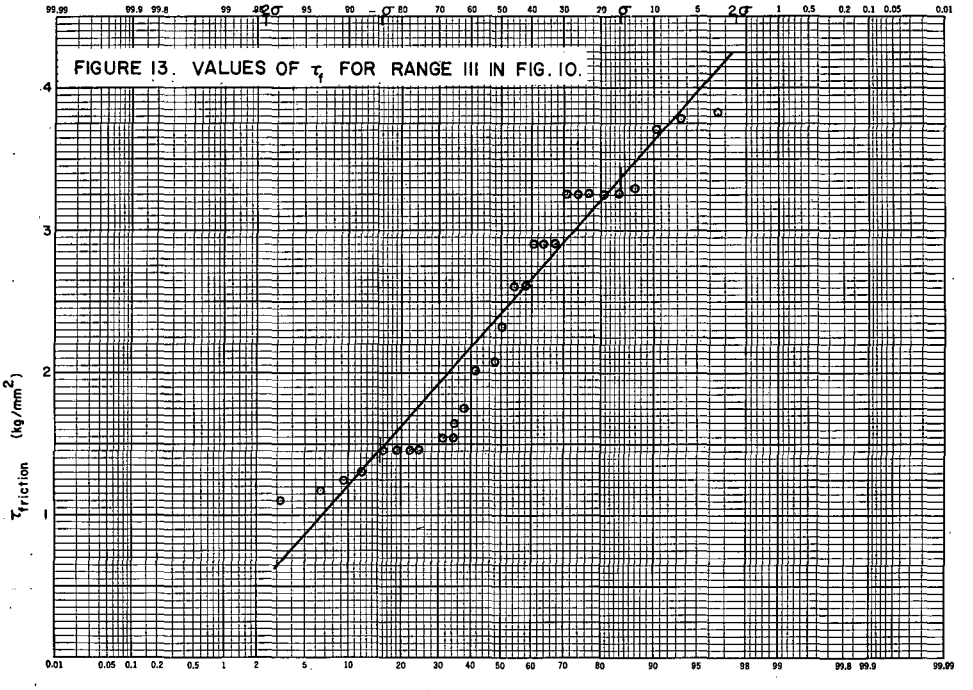

FIGURE 13. VALUES OF τ_f FOR RANGE III IN FIG. 10.

MU-27855

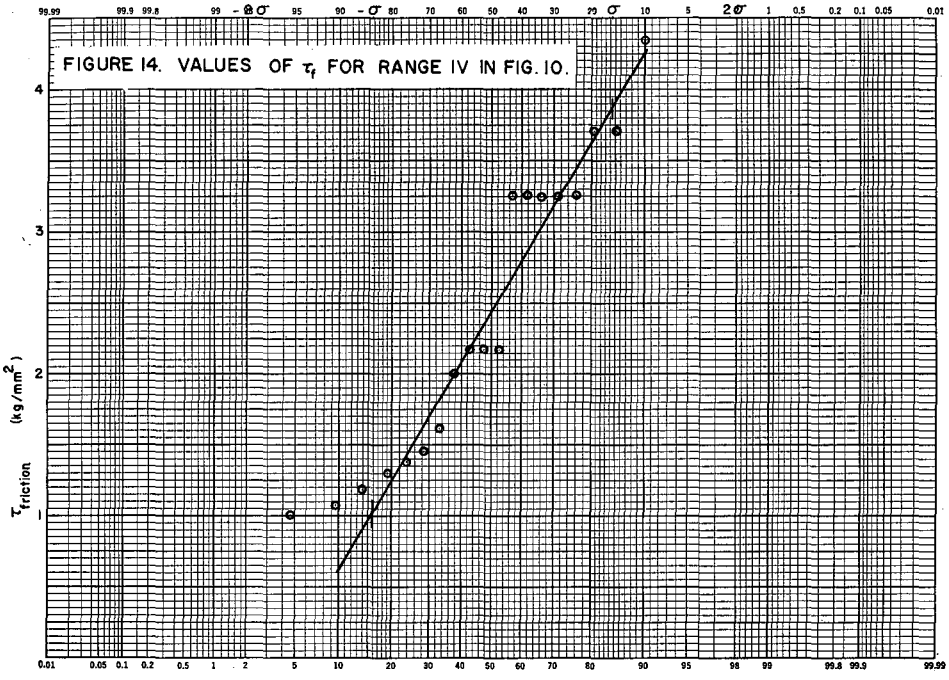

FIGURE 14. VALUES OF τ_f FOR RANGE IV IN FIG. 10.

MU-27856

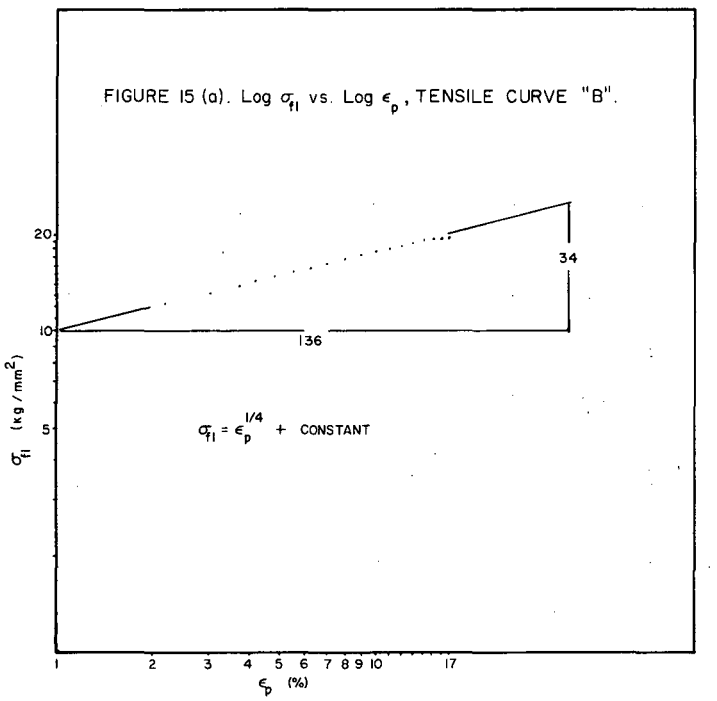

FIGURE 15 (a). Log σ_{fl} vs. Log ϵ_p, TENSILE CURVE "B".

MU-27857

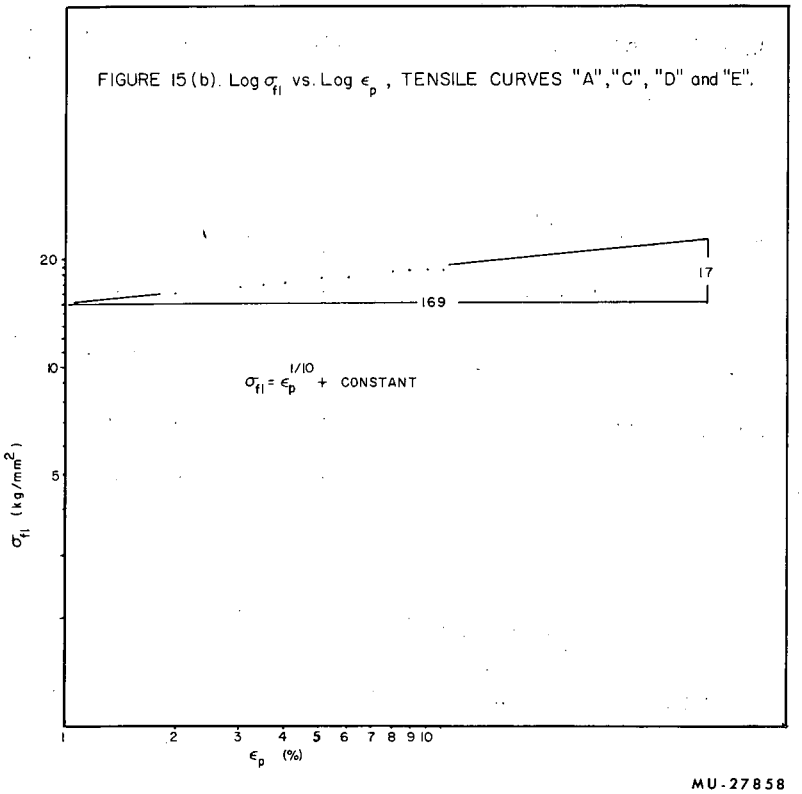

FIGURE 15 (b). Log σ_{fl} vs. Log ϵ_p , TENSILE CURVES "A", "C", "D" and "E".

MU-27858

In exponential form the relation is:

$$\sigma_{fl} = \epsilon_p^{\frac{1}{10}} + \text{constant.}$$

In Fig. 15(a) and 15(b) the points diverge from the straight line at the higher stress values. The point of divergence indicates where the true stress is not well approximated by the stress calculated by dividing the instantaneous load by the original cross section of the specimen [14].

4.2 Dislocation Density

In order to determine the relationship between the dislocation density, flow stress and plastic strain, the same log-log method used for the relations between observed stress and strain was employed. The functional relation between dislocation density and flow stress for tensile curve type "B" is:

$$\sigma_{fl} \left(\frac{kg}{cm^2}\right) = 0.85\ Gb\rho^{\frac{1}{2}} + \text{constant.}$$

The corresponding relation between plastic strain and dislocation density is:

$$\epsilon_p(\%) = 5.3 \times 10^{-20}\ \rho^2 + \text{constant.}$$

The values of the coefficients were determined by a linear least squares analysis of the average points of $\rho^{\frac{1}{2}}$ versus σ_{fl} and ρ^2 versus ϵ_p as shown in Fig. 16 and 17. The total range of ρ and the average of the range are shown.

It has been shown above that the flow stress, σ_{fl} for tensile curve "B" can be expressed in terms of the dislocation density by the relation:

$$\sigma_{fl} = A\rho^{\frac{1}{2}} + \text{constant}$$

where A is a constant for a given condition. The plastic strain for

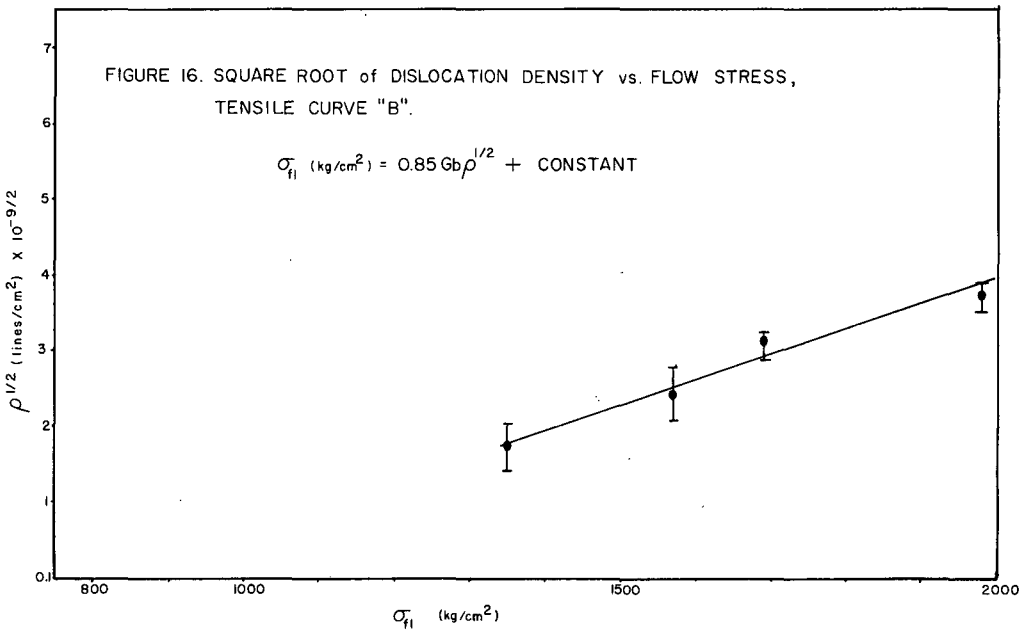
FIGURE 16. SQUARE ROOT of DISLOCATION DENSITY vs. FLOW STRESS, TENSILE CURVE "B".
σ_{fl} (kg/cm^2) = 0.85 Gb$\rho^{1/2}$ + CONSTANT
$\rho^{1/2}$ (lines/cm^2) X 10$^{-9/2}$
7
6
5
4
3
2
1
0.1
800
1000
1500
2000
σ_{fl} (kg/cm^2)
MU-27859

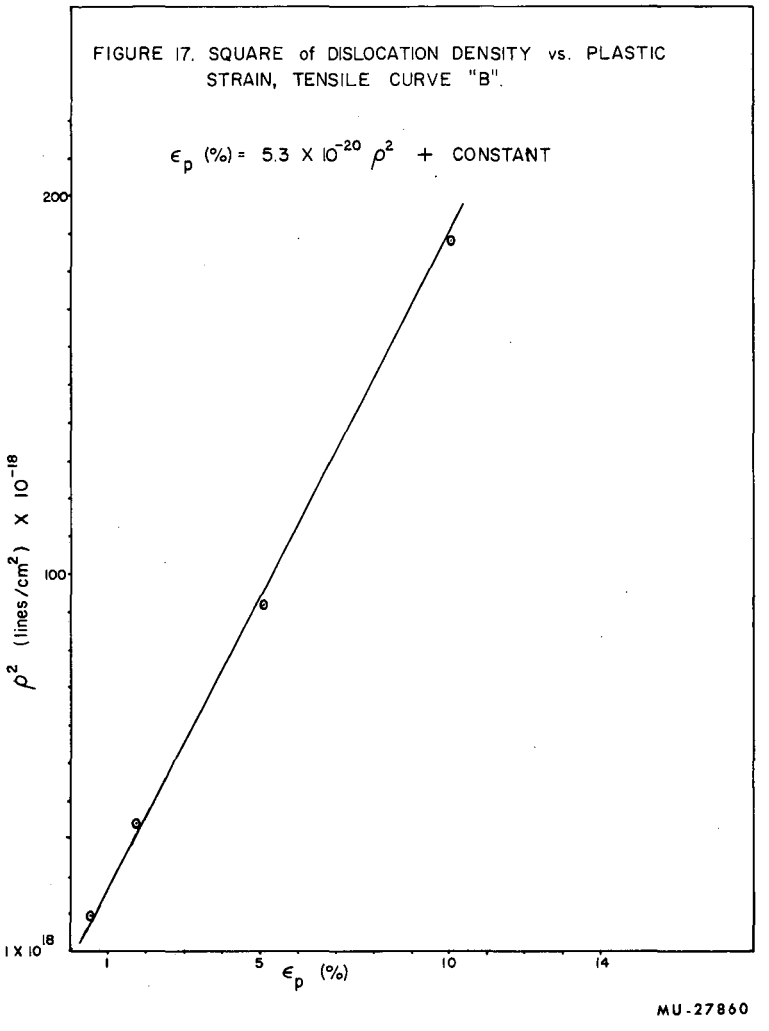

FIGURE 17. SQUARE of DISLOCATION DENSITY vs. PLASTIC STRAIN, TENSILE CURVE "B".

this type tensile curve can also be expressed in terms of the dislocation density by the relation:

$$\epsilon_p = B\rho^2 + \text{constant}$$

where B is a constant.

Clearly from these two relations, obtained from dislocation density measurements, a relation between σ_{fl} and ϵ_p can be obtained. The two above expressions give:

$$\sigma_{fl} = C\epsilon_p^{\frac{1}{4}} \qquad \text{where C is a constant.}$$

This is the same functional relation between σ_{fl} and ϵ_p obtained from the experimental tensile curve. Hence, the relations between σ_{fl} and ϵ_p, obtained from dislocation density measurements, correlate with the functional relation between σ_{fl} and ϵ_p obtained from the experimental tensile curve "B".

Since the observed flow stress-plastic strain functional relations are very different for the two types of tensile curves, the functional relation between flow stress and plastic strain with dislocation density would likewise be expected to be different. By applying the same log-log methods as above, the functional relation between flow stress and dislocation density for tensile curve "C" was found to be from Fig. 18(a)

$$\sigma_{fl}\ (\tfrac{kg}{cm^2}) = 6.5 \times 10^3\ Gb\rho^{\frac{1}{7}} + \text{constant.}$$

The relation between plastic strain and density is from Fig. 18(b)

$$\epsilon_p\ (\%) = 2.52 \times 10^{11}\ \rho^{\frac{1}{7}} + \text{constant.}$$

The values of the coefficients were determined by a linear least squares analysis of $\rho^{\frac{1}{7}}$ versus σ_{fl} and $\rho^{\frac{10}{7}}$ versus ϵ_p as shown in Fig. 19 and 20. The total range of ρ and the average of the range are shown.

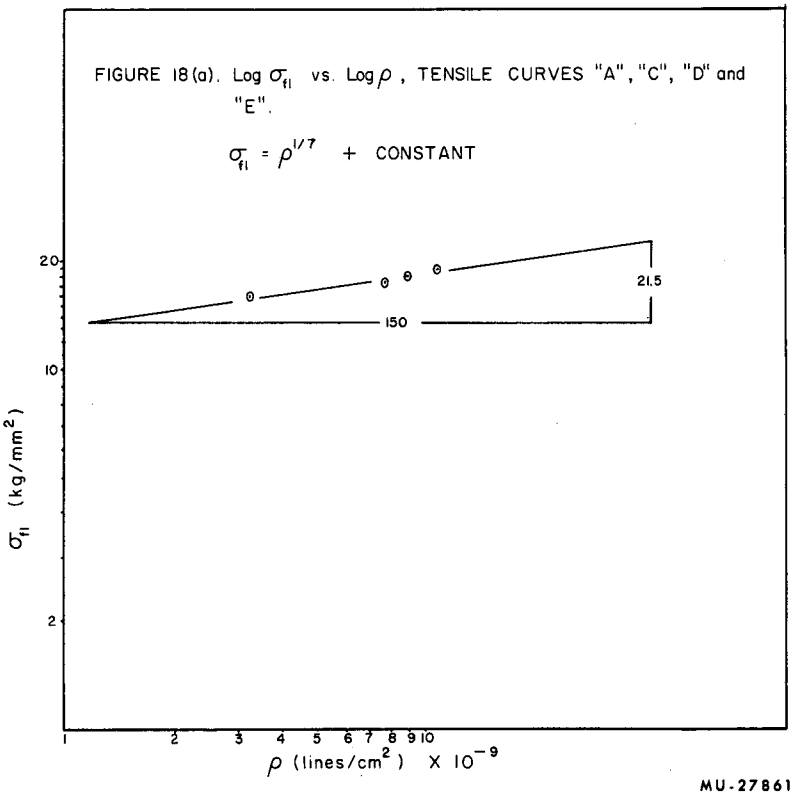
FIGURE 18(a). Log σ_{fl} vs. Log ρ, TENSILE CURVES "A", "C", "D" and "E".
$\sigma_{fl} = \rho^{1/7}$ + CONSTANT
0
0
0
0
21.5
150
20
10
2
σ_{fl} (kg/mm^2)
1
2
3
4
5
6
7
8
9
10
ρ (lines/cm^2) X 10^{-9}
MU-27861

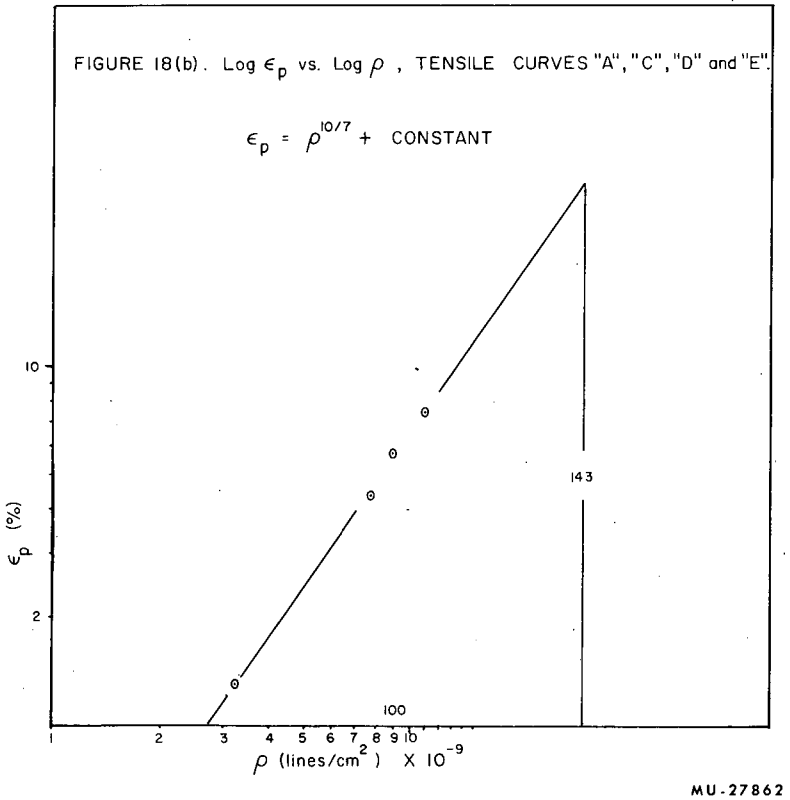

FIGURE 18(b). Log ϵ_p vs. Log ρ , TENSILE CURVES "A", "C", "D" and "E".

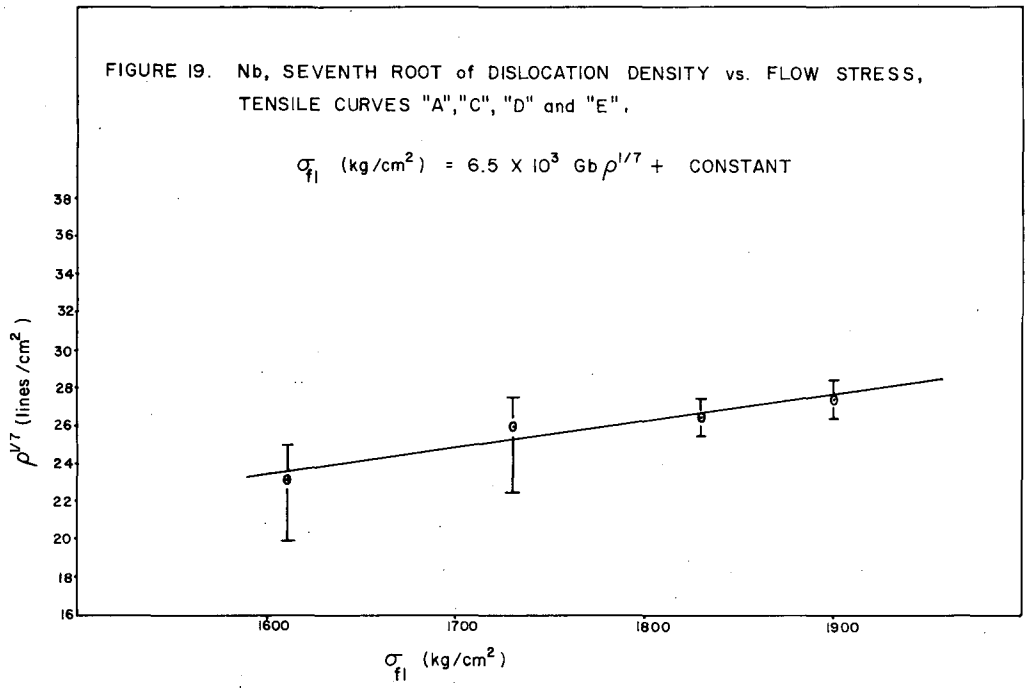

FIGURE 19. Nb, SEVENTH ROOT of DISLOCATION DENSITY vs. FLOW STRESS, TENSILE CURVES "A","C", "D" and "E".

MU-27863

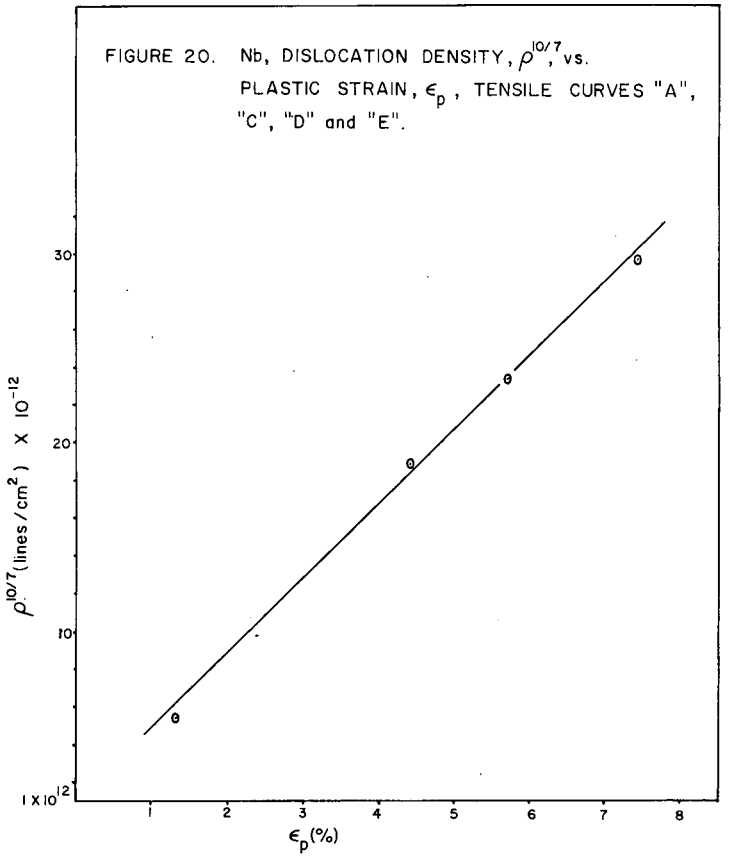

FIGURE 20. Nb, DISLOCATION DENSITY, $\rho^{10/7}$, vs. PLASTIC STRAIN, ϵ_p, TENSILE CURVES "A", "C", "D" and "E".

The range of ρ is larger at lower σ_{fl} due to inhomogeneous deformation at this stress level. The bottom of the range represents ρ in front of the Luders band front and the top of the range represents ρ behind the Luders band front.

The observed stress-strain functional relation for tensile curve type "C" can also be derived from dislocation density versus flow stress and versus plastic strain relations. The result is:

$$\sigma_{fl} = C\epsilon_{p}^{\frac{1}{2}} \qquad \text{where C is a constant.}$$

Hence, there is excellent correlation with dislocation density and the observed flow stress-strain relation for tensile curve type "C" and similar ones, i.e., "A", "D" and "E".

4.3 Grain Size Effect on Yield Strength

Various grain sizes were obtained by the annealing cycles employed. When τ_{ly} was plotted versus grain size, as in Fig. 21, no discernable relation was observed. However, when a plot of τ_{ly} versus impurity content is made, a linear relation of positive slope is obtained. The effect of grain size on τ_{ly} has been observed to be relatively small in Nb[10]. Therefore τ_{ly} is influenced by the dislocation substructure far more than by grain size. The dislocation substructure is very dependent on the impurity content and annealing history of the specimen. Hence, if the impurity content changes from one grain size to another, the effect of grain size on τ_{ly} will be masked by changes in the dislocation substructure concomitant with changes in impurity level. It should be pointed out therefore that the method of varying grain size by heat treatments in Nb should be done with utmost caution since it is almost

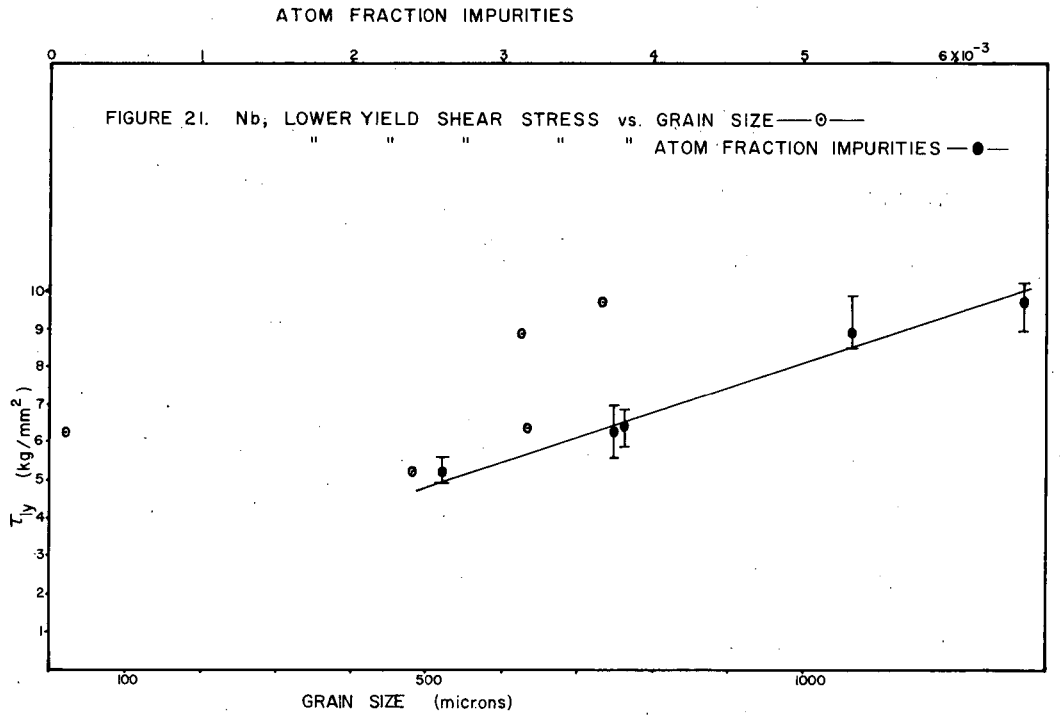
ATOM FRACTION IMPURITIES
0
1
2
3
4
5
6X10⁻³
FIGURE 21. Nb; LOWER YIELD SHEAR STRESS vs. GRAIN SIZE —⊙—
" " " " " ATOM FRACTION IMPURITIES —●—
τly (kg/mm²)
10
9
8
7
6
5
4
3
2
1
100
500
1000
GRAIN SIZE (microns)
MU-27865

impossible to heat treat Nb without changing the impurity content and/or the manner in which it appears within the specimen.

5 Discussion of Results

5.1 Microstrain

Microstrain is considered here to be the plastic strain that occurs in the specimen between the elastic limit and the upper yield point, σ_{uy}, on the tensile curve, as shown in Fig. 5. The microstrain is thought to occur by the motion of a relatively small number of mobile dislocations in the specimen.

The origin of the dislocations contributing to the microstrain can occur by two similar processes. Cottrell and Bilby[14] originally proposed that upon loading a BCC crystal, dislocations at regions of stress concentration would become unlocked from atmospheres of solute atoms or small precipitates and then move through the crystal. These mobile dislocations would move until they encountered barriers such as subgrain boundaries and there form a pileup. The long range stress field of the pileup would activate a dislocation source at some distance from the barrier. As the frequency of such events increases with increasing stress the crystal becomes flooded with dislocations at the upper yield point. The likely source of dislocations causing microstrain is thought to occur in the following manner. Dislocation sources become activated at the junction between the specimen and the tensile grips since the act of gripping the specimen causes plastic deformation at the junction. These mobile dislocations multiply by a cross-slip mechanism increasing the amount of strain. The Luders

bands in Fig. 8 originate from this junction, which tends to support such a mechanism. Although the concept of dislocation unlocking is appealing, the pileup mechanism of the process seems unlikely since classical pileups of dislocations have not been observed in any of the more than one hundred Nb specimens examined in the electron microscope. Furthermore, other workers have not observed them in Fe[16] or Mo[1].

5.2 Upper Yield Point

The upper yield point is considered here as being the stress at the first point of tangency beyond the elastic limit of a horizontal line with the tensile curve as shown in Fig. 5. In BCC metals the upper yield point is sometimes considered as a discontinuity in the tensile curve. However, as can be seen in Fig. 6, the stress-strain curve changes shape continuously at the upper yield point.

The upper yield point is probably one of the most interesting features of the Nb tensile curve. Johnston[17] has presented a plausable mechanism to explain the upper yield point and the yield drop in single crystals. The plastic strain rate in the absence of work hardening can be expressed by:

$$\dot{\epsilon}_p = bn(\alpha\epsilon)\, v(\tau)$$

where b = the burgers vector

$n(\alpha\epsilon)$ = number of mobile dislocation which is a function of α and ϵ

α = the dislocation multiplication rate

ϵ = the plastic strain (in Nb beyond σ_{1y})

$n = \alpha\epsilon^{\frac{1}{2}}$, for curve "B" and $n = \alpha\epsilon^{\frac{7}{10}}$ for curve "C" (near the yield point it is not certain that these exponents apply)

$v(\tau)$ = the dislocation velocity, which is a function of the shear stress τ.

The shape of the stress-strain curve near σ_{uy} is thought to be produced by the following sequence of events. As the stress on the specimen is increased appoaching the elastic limit a few mobile dislocations have begun to move and at the elastic limit some have passed through the crystal. The location of the elastic limit is of course dependent on the ability to measure small strains. At higher stresses, approaching σ_{uy}, dislocations are probably moving very rapidly. Although the dislocations have high velocities, the number that are moving is such that the inequality:

$$\dot{\epsilon}_p = bn(\alpha, \epsilon)\, v(\tau) \ll \frac{V_{ch}}{L_o}$$

is satisfied. Here V_{ch} is the velocity of the tensile machine crosshead and L_o is the specimen gauge length. It is also assumed here that the testing machine is perfectly elastically hard. This is a valid assumption when comparing the geometry of the testing machine with the specimen geometry used here. However, dislocation multiplication is occurring and eventually there exists a sufficient number of dislocations so that the equality:

$$bn(\alpha, \epsilon)\, v(\tau) = \frac{V_{ch}}{L_o}$$

is attained and the stress-strain curve levels off at σ_{uy}. Beyond σ_{uy} the strain increases, the number of dislocations increases, their average velocity decreases and the stress decreases. If dislocation barriers and interactions are absent in the specimen, i.e., there is no work hardening, the stress would continue to decrease to zero.

Dislocation density measurements at σ_{uy} and just approaching σ_{ly} showed that a high rate of dislocation multiplication does occur in this portion of the stress-strain curve. In areas of the specimens where

dislocation motion had occurred, e.g., Fig. 22 and 23, the average dislocation densities determined from five foils at σ_{uy} and five foils at σ_{ly} from random regions of the specimens were:

$$\text{at } \sigma_{uy}, \qquad 8.64 \times 10^8 (\text{lines/cm}^2)$$

$$\text{at } \sigma_{ly}, \qquad 29.8 \times 10^8 (\text{lines/cm}^2) .$$

This is an increase in dislocation density by a factor of about three. For an equivalent increment in strain beyond σ_{ly}, i.e., an amount equal to $\epsilon\,(\sigma_{ly}) - \epsilon\,(\sigma_{uy})$, the change in dislocation density is:

$$(16.3 \times 10^8 - 11.7 \times 10^8) \ \text{lines/cm}^2.$$

Therefore the dislocation multiplication rate is greater near the yield points than the rate occurring beyond σ_{ly}.

Since the amount of yield drop depends on the number of mobile dislocations initially present, σ_{uy} is somewhat difficult to reproduce from one specimen to another. σ_{uy} is very sensitive to specimen alignment because any compound loading placed on the specimen such as bending prior to or during the initial loading generates large numbers of mobile dislocations which will tend to mask the upper yield point.

5.3 Lower Yield Point

The lower yield stress, σ_{ly}, is here considered to be the stress at the tangent point of a horizontal line with the stress-strain curve shown in Fig. 5.

Petch[4] has shown in polycrystalline Fe and steel, that the lower yield point can be expressed by the empyrical relation:

$$\tau_{ly} = \tau_{friction} + K^*/d^{\frac{1}{2}}$$

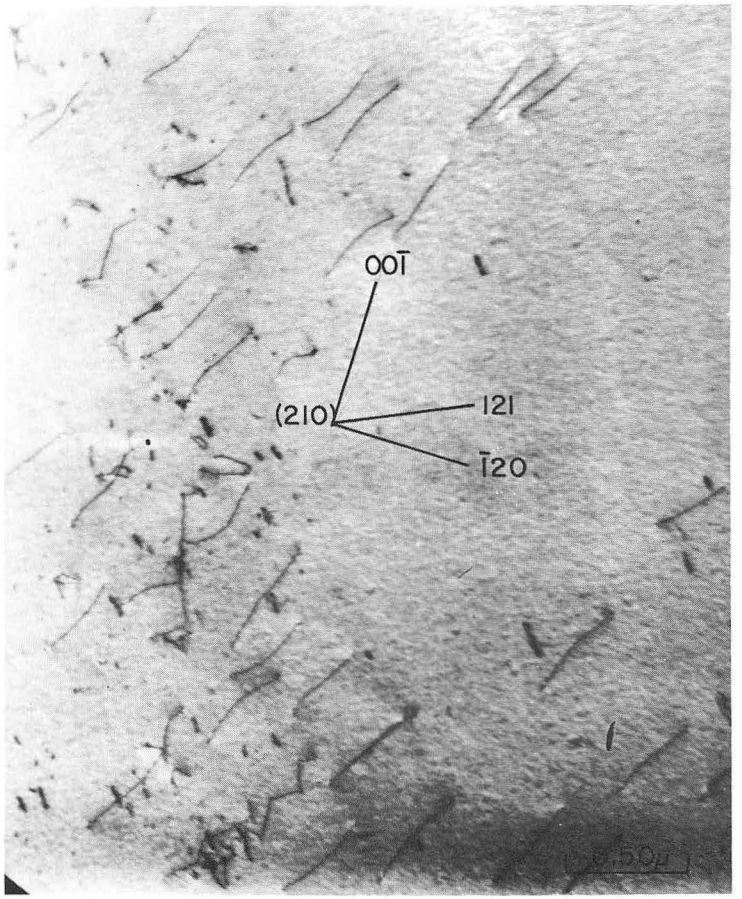

FIGURE 22. TYPICAL DISLOCATION DENSITY at σ_{uy}

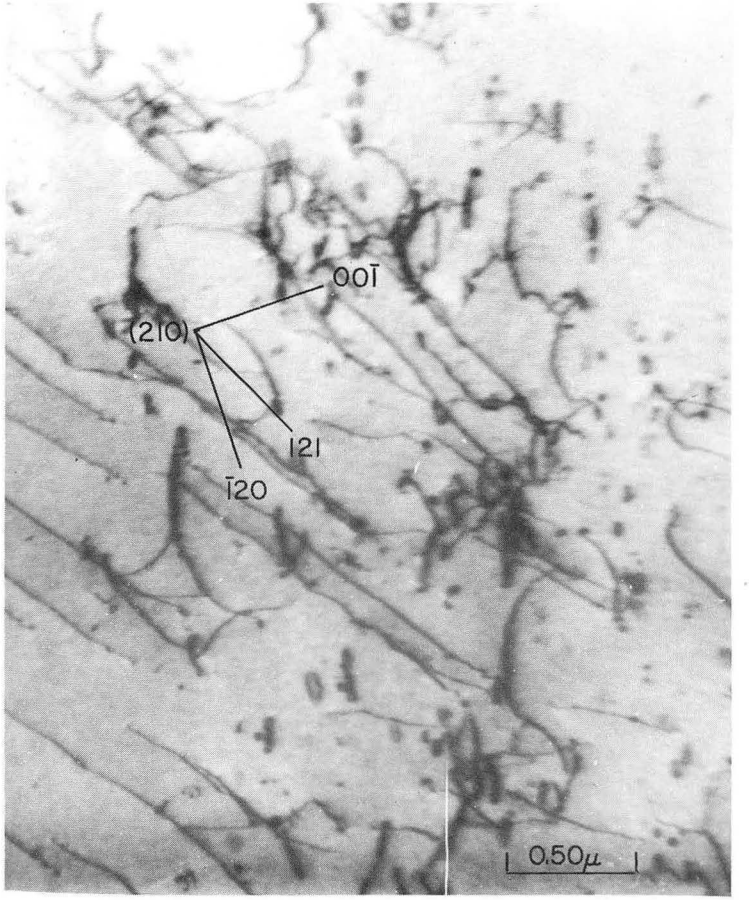

FIGURE 23. TYPICAL DISLOCATION DENSITY APPROACHING σ_{ly}

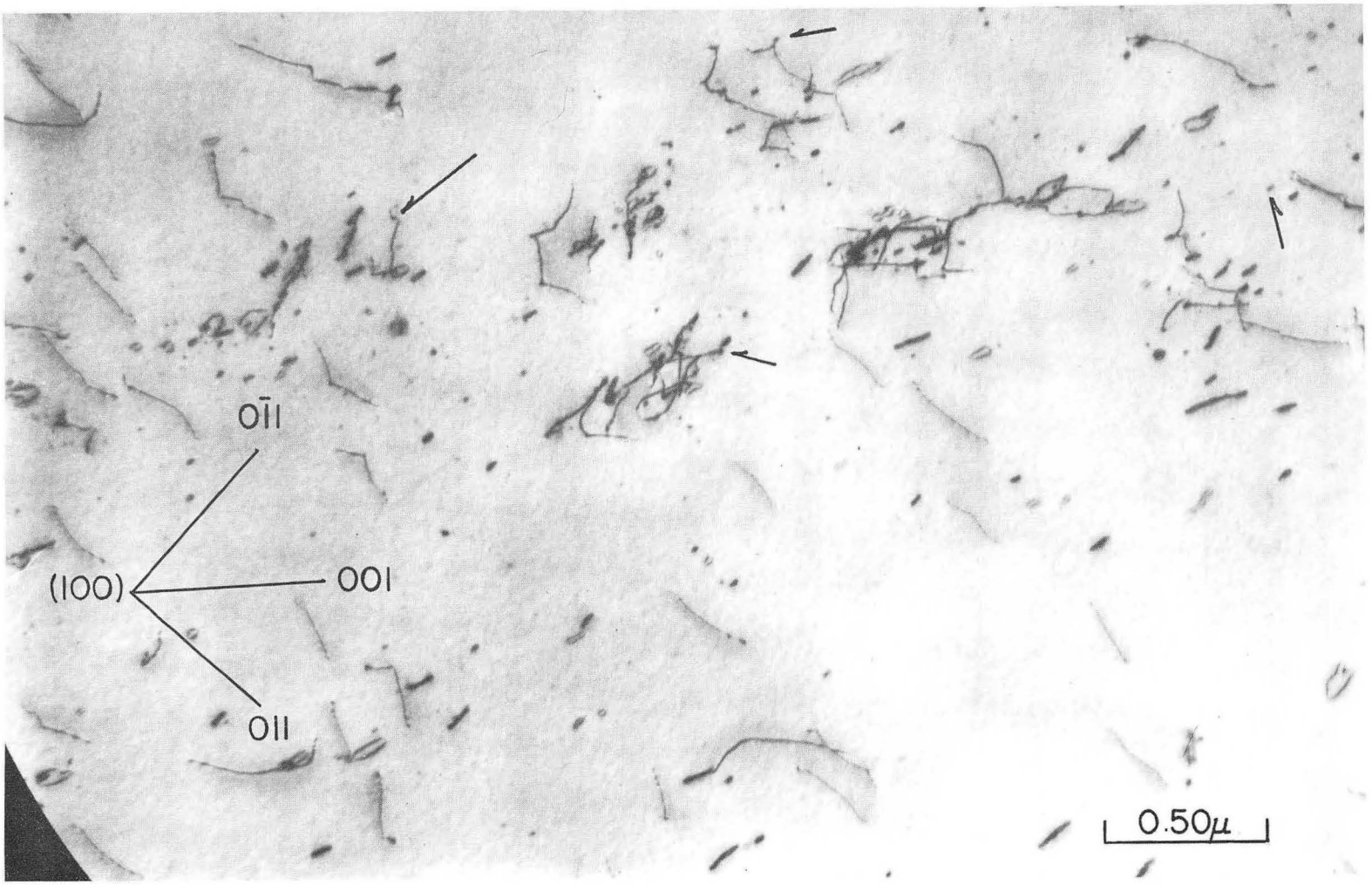

FIGURE 24. SOLUTE ATOM CLUSTERS or SMALL PRECIPITATES as DISLOCATION BARRIERS.

ZN-3229

where $\tau_{friction}$ = a friction stress retarding the motion of a dislocation in the crystal lattice

K^* = a parameter for the given metal

d = the average grain diameter.

This relation is also supposed to be valid for τ_{uy} and the flow stress. Other investigations[10, 18, 19, 20, 21] have applied a Petch analysis to determine K^* for Nb. However, there is some disagreement in the value of K^* between these investigations. It is quite obvious from Fig. 21 that such an analysis could not be made for the specimens here. A change in grain size was concomitant with changes in the impurity content with the anneals used to obtain the changes in grain sizes. The disagreement in the values obtained for K^*, therefore, are probably due to differences in impurity level.

Yielding of a crystal is influenced by the ease with which dislocations can move through it. The motion of a dislocation is influenced by any barrier that may lie in its path. Here, the shear stress required to move dislocations through a crystal containing such barriers will be denoted by $\tau_{structure}$. Structure refers to anything excluding lattice friction that impedes the motion of the dislocations. Hence, the lower yield stress can be expressed by:

$$\tau_{ly} = \tau_{friction} + \tau_{structure}.$$

An indication of the magnitude of τ_f was obtained by measuring the radius of 118 isolated curved dislocations. The dislocation curvature is assumed to be due to the atomic lattice-dislocation and solute atom-dislocation interaction or dislocation jogs that are not resolved.

Since the solute atoms interacting with the dislocation are dispersed below the limit of resolution of the electron microscope, they are here considered to be in solution. The friction stress can be expressed by:

$$\tau_f = \frac{Gb}{r}$$

where $r = (\frac{4}{\pi}) r_p$ = radius of curvature

r_p = projected radius on the micrograph

$(\frac{4}{\pi})$ = a factor applied when assuming r_p to be randomly oriented.

A plot of τ_f versus atom fraction of impurities appears in Fig. 10. The mean points and the limits of each range are determined by making a probability plot for the measured values of τ_f corresponding to a given purity level. The probability plots corresponding to the ranges I, II, III and IV in Fig. 10 are shown in Fig. 11, 12, 13 and 14. It is clearly evident that these plots give one standard deviation directly and a second standard deviation can be obtained by a very short extrapolation of the line. The least squares line through the mean points of τ_f has a slight positive slope. Such a result implies that τ_f has some dependence on the amount of impurity atoms in solution. It should be made clear that the term "in solution" here means the solute atoms are not clustered or in a precipitate phase large enough to be resolved in the microscope. Since τ_f shows some dependence on impurity content, it seems reasonable to factor τ_f into two terms, given by:

$$\tau_f = \tau_o + \tau_{soln.}$$

where τ_o = lattice friction of a pure crystal

$\tau_{soln.}$ = the friction contribution due to impurities in solution

τ_o could be due to a Peierls-Nabarro force on a dislocation. If it is, then τ_o would be expected to be temperature dependent and would contribute to the temperature dependence of τ_{ly}.

If it is assumed that a linear relation between τ_f and atom fraction of impurities is valid for impurity levels approaching zero, an extrapolation of the line to zero impurities will give an estimate of τ_o. Such an extrapolation gives a value of τ_o of about 0.8 $(\frac{kg}{mm^2})$. This would be a maximum value since the curve of the mean points shows a tendency to nonlinearity at the lower impurity levels.

The contribution of $\tau_{structure}$ to τ_{ly} is relatively large compared to τ_f. $\tau_{structure}$ is the contribution due to barriers in the crystal that impede the motion of dislocations. The dislocation barriers that have been observed in Nb will now be discussed.

Plates of precipitate have been observed on dislocations that are in the form of a network. These plates are shown at A in Fig. 7. These networks, which the precipitate plates nucleate on and grow from, have only been observed in the specimens annealed at 1000°C. This is the group that produces tensile curve "B" in Fig. 6.

At higher annealing temperatures dislocation networks have not been observed. Dislocations can be seen interacting with these plates at "B" in Fig. 7.

Precipitate plates large enough to obtain a selected area diffraction pattern have not yet been observed. However, these plates are thought to be some form of Nb carbide. This is based on internal friction measurements of the carbon peak in Nb made by Powers and Doyle[22]. They found that the carbon peak decreased as the number of aging treatments

increased. This suggests that the carbon is involved in the precipitation of some second phase or is clustering. Furthermore, similar appearing precipitate plates on dislocations have been observed by Keh and Leslie[23] in an aged Fe-Si-C alloy, and were identified as a carbide.

The most obvious barrier to the motion of dislocations observed in specimens annealed at all the temperatures, including 1000°C, is the presence of very small, nearly spherical particles, the contrast from which is sensitive to specimen orientation. These barriers together with dislocations interacting with them can be seen in Fig 24. Further, clusters associated with dislocations can be resolved by tilting dislocations out of contrast. The measured diameter of these particles ranges from 50 to 150Å. A bright field image of a (112) foil together with a $(\bar{1}10)$ dark field image of the same area is shown in Fig. 25 (b) and (c). It can be observed that the contrast from some of these specks arises from the $(\bar{1}10)$ reflection. Note the bright spots in the dark field image that correspond to dark spots in the bright field image. Hence, it is thought that these particles are due to clustering of solute atoms on the {110} planes of the Nb crystal. It is not thought that the contrast arises solely from dislocation loops or dislocations perpendicular to the foil surface. These particles can be seen in Fig. 25 (a) in a fully annealed undeformed specimen. Clearly there are no dislocation loops associated with them. In Fig 25 (b) the contrast is greatest on one end of the elongated loop, indicating that the loop is pinned on one side. In Fig. 25 (c) the maximum brightness in the dark field corresponds to the pinned side of the loop and the pinned end of the dislocation line. Such observations indicate that the particles are

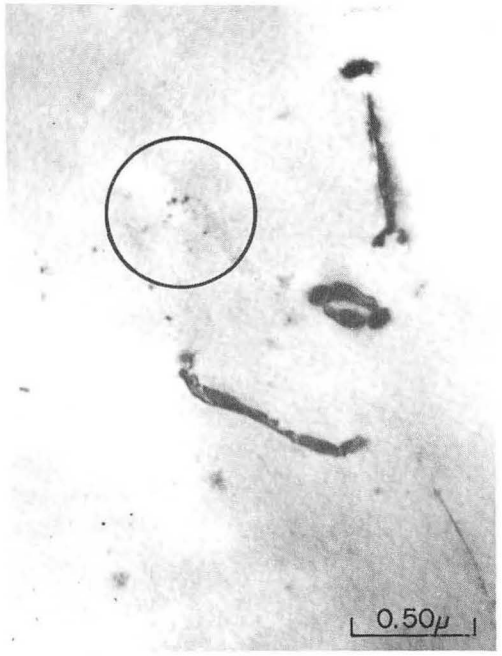

(a). ANNEALED, (111).

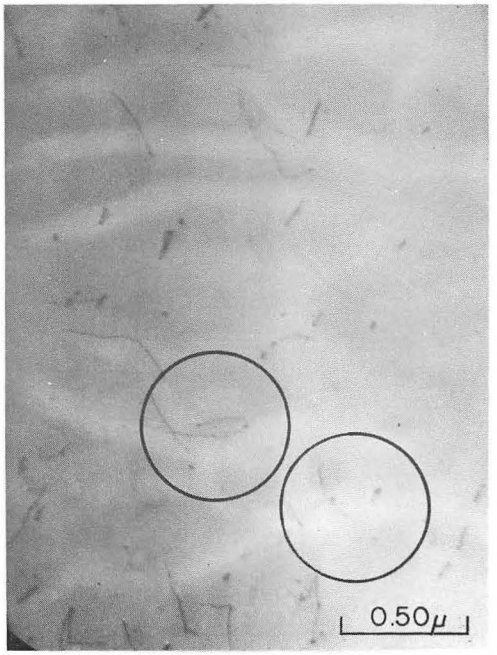

(b). ϵ_p=0.2%, (112) BRIGHT FIELD.

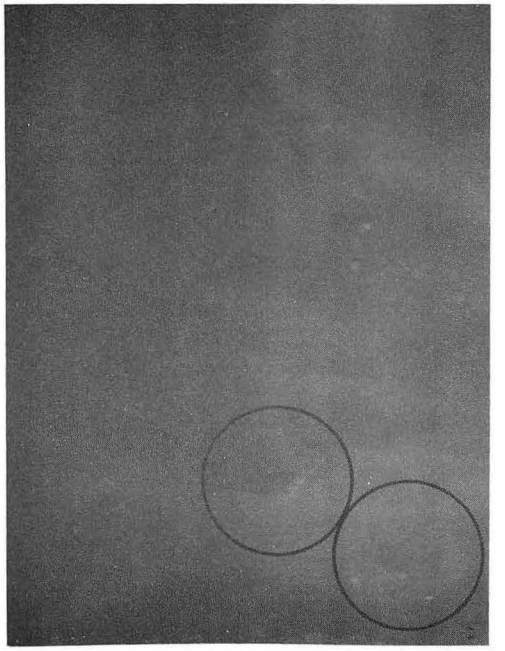

(c). ($\bar{1}$10) DARK FIELD of (b).

FIGURE 25. SOLUTE ATOM CLUSTERS and DISLOCATIONS.

ZN-3230

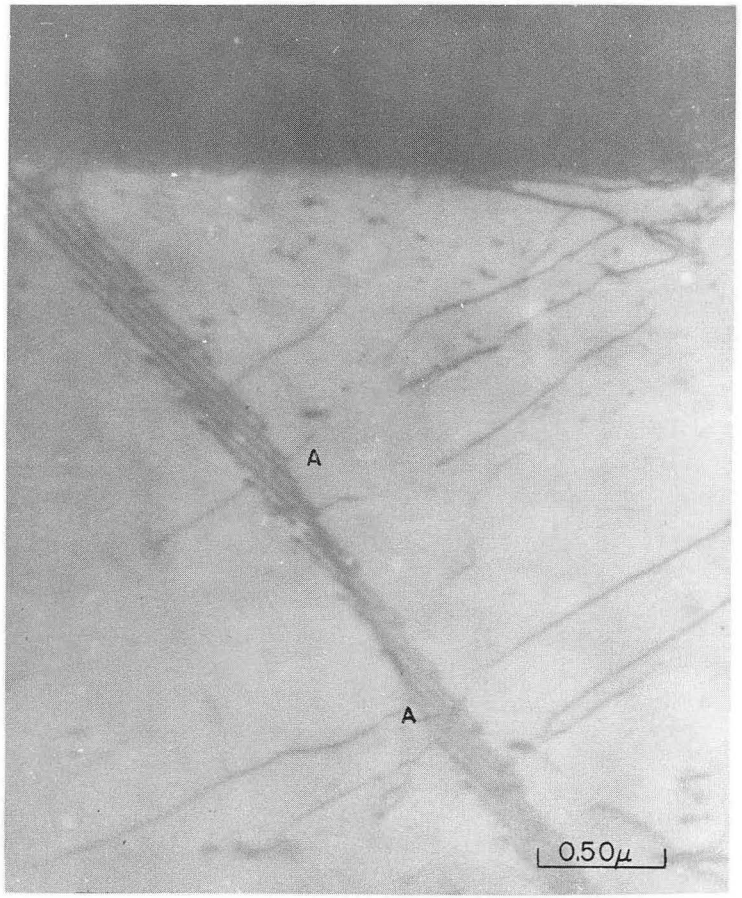

(a). DISLOCATION, A–A, AGAINST A TILT BOUNDARY

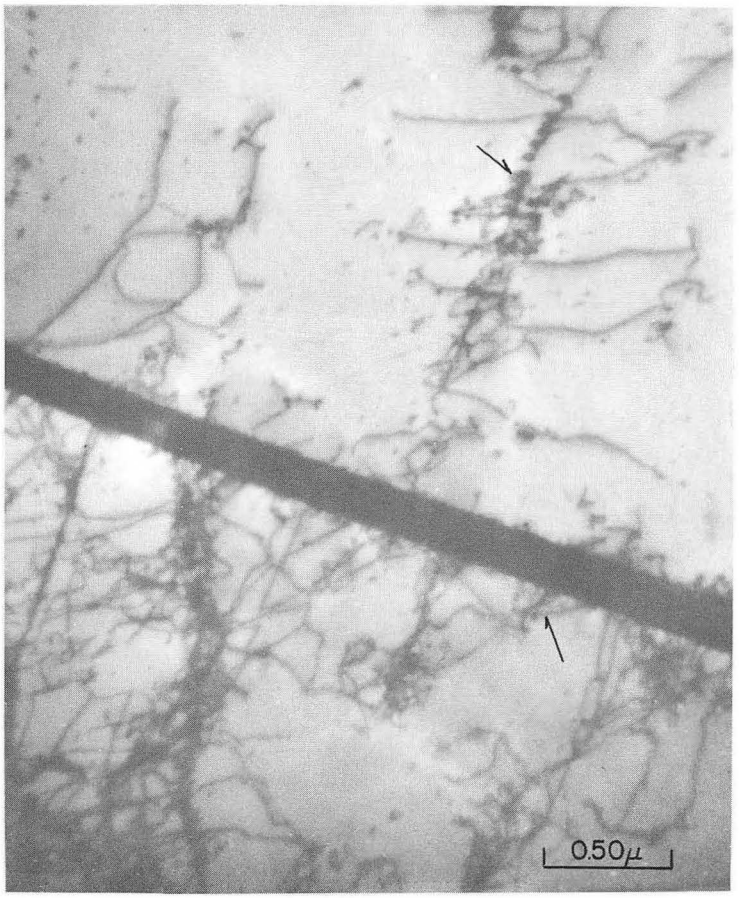

(b). DISLOCATIONS INTERACTING with A GRAIN BOUNDARY, and PRECIPITATES.

FIGURE 26.

making the maximum contribution to the contrast. The most likely solute atoms that would cluster would be those that have the large $|\epsilon|$. From Table 3, these would be the interstitials carbon, oxygen, nitrogen and hydrogen. The two likely metallic impurities are silicon and iron. It should be remarked that ϵ considers only the relative geometry of the solute atom and any other effects such as electronic interactions between atoms have not been considered.

Crystal boundaries will also impede the motion of dislocations. In Fig. 26 (a) a dislocation marked A-A is seen to be against a simple tilt boundary. In Fig. 26 (b) many dislocations are seen to be interacting with the boundary and with precipitates.

A linear relation was observed between τ_{ly} and impurity content as shown in Fig. 9. The same linear relationship is desired for the yield strength when the movement of dislocations through the crystal is considered. Cottrell[9] has discussed a mechanism proposed by Mott and Nabarro that yields a linear dependence of τ_{yield} on impurity content. A crystal containing isolated and clusters of solute atoms will be subjected to internal strain fields at these points.

An interesting aspect of the clustering of the solute atoms is that the degree of misfit is independent of the size of the cluster. This follows since any spherical region in the crystal which encloses a given group of sites changes its radius by the factor $(1 + \epsilon)$ when solvent atoms in these sites are replaced by solute atoms. Elasticity theory shows that the shear strain at a distance R from a spherical cluster of radius r_o and misfit ϵ is given by:

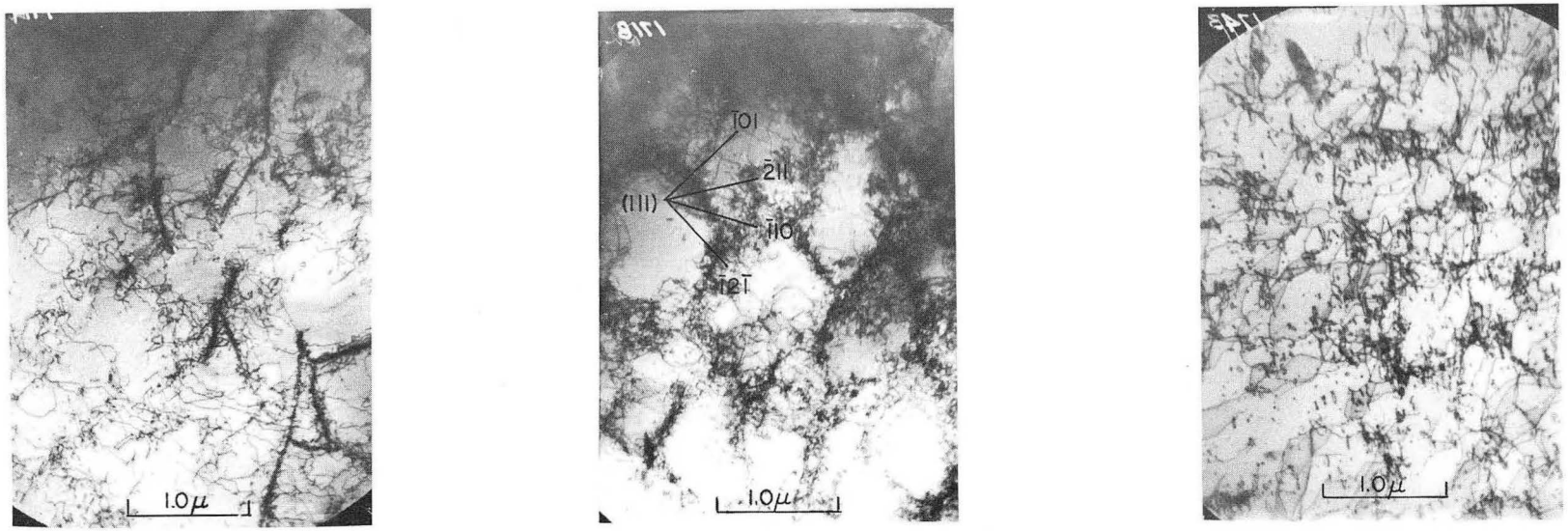

(a) (b) (c)

FIGURE 27. TYPICAL DISLOCATION SUBSTRUCTURE at ϵ_p = 10%.
(a) and (b) SUBSTRUCTURE in SPECIMENS GIVING TENSILE CURVE "B",
(c) SUBSTRUCTURE in SPECIMENS GIVING TENSILE CURVES "A", "C", "D" and "E".

ZN-3232

$$\frac{\epsilon r_o^3}{R^3} \quad , \quad \text{valid for } R > r_o .$$

Hence, changes in the state of dispersion, without changes in ϵ, alter only the wavelength of the internal stresses and not their amplitude. When the dispersion of these internal strain centers is such that the wavelength of the internal stress field is small compared to the limiting radius of curvature of a dislocation, i.e.,

$$\lambda < \frac{Gb}{\tau_{yield}} .$$

Nabarro has shown that the yield strength of a polycrystalline specimen is approximated by the expression:

$$\tau = G \epsilon^2 c .$$

Here λ = wavelength

τ_{yield} = observed yield stress

ϵ = misfit parameter

c = concentration of impurity

τ = yield strength predicted by the model .

The observed values of λ in the specimens show that the above inequality is satisfied.

The calculated values of τ, from the above expression, obtained for the various levels of impurities are shown in the lower curve of Fig. 9. A least squares line has been drawn for these points. It is assumed:

$$\tau = G \epsilon^2 c \doteq \tau_{structure} .$$

The slope of the $\tau_{structure}$ line is nearly parallel to the observed

τ_{ly} line, which is encouraging. However, $\tau_{structure}$ obtained from the expression:

$$\tau_{st} = G \epsilon^2 c$$

should pass through the origin when c is equal to zero. Possible reasons why the line does not pass through the origin are errors in the determination of G and c as well as assumptions inherent in atomic radii in the calculation of ϵ. Since there is a constant difference in the line, the error probably is in the chemical analysis c.

Previously it was assumed that the lower yield stress could be expressed by:

$$\tau_{ly} = \tau_f + \tau_{structure}:$$

If the values of τ_f from Fig. 10 are added to τ_{st} the dashed line in Fig. 9 is obtained. The significance of the dashed line is that the slope is in excellent agreement with the slope of observed τ_{ly}. The constant difference in the two lines can be removed by shifting the $\tau_{structure}$ line so that it passes through the origin as it should at c equal to zero. On the other hand, the observed τ_{ly} line was obtained at a fixed strain rate and changes in strain rate will raise and lower the yield point. For example, the specimens whose average τ_{ly} is marked by a pyramid in Fig. 9 were strained at a strain rate one tenth less than the specimens in the range immediately above. Notice that τ_{ly} for $\frac{\dot{\epsilon}}{10}$ cluster on the dashed line. The effect of an increase in strain rate is to magnify the stress strain curve[17]. Hence, the real significance is that the observed τ_{ly} line is parallel to τ_{ly} obtained from measured τ_f and $\tau_{structure}$ based on the dilation imposed by solute atom clusters.

5.4 Flow Stress

Tensile flow stress, σ_{fl}, is considered here to be the value of tensile stress on the stress strain curve at increments of strain beyond the lower yield point.

It is quite obvious from Fig. 6 that the flow stress in curve "B" is very different from the flow stress in the specimens exhibiting the tensile curves "A", "C", "D" and "E". Reasons for this behavior can be derived from a comparison of the dislocation substructures in the different specimens.

The formation of a well-defined cell structure in deformed metals has been observed by other investigators[7, 16]. The boundaries of the cells are composed of very dense regions of dislocations surrounding relatively dislocation-free areas. Fig. 27 (a) and (b) show dislocation substructure developed in specimens having a tensile curve of type "B" compared to the substructure developed in specimens having a tensile curve of type "C", as shown in Fig. 27 (c). The specimens of Fig. 27 (a) and (b) have developed a well-defined cell structure as compared to that in Fig. 27 (c). In Fig. 27 (a) and (b) the cell structure has developed from dislocation tangles formed at the precipitate plates existing on the original dislocations. There were no dislocation networks observed in the specimens represented by the substructure shown in (c). Furthermore, specimens showing a tensile curve of type "C" have been deformed to about 22 percent elongation without observing any dislocation cell structure formation.

It is likely that much more severe deformation is required to develop a cell structure in Nb when the specimen is deformed at room

temperature. However, Keh and Weissmann[16] have observed a temperature dependence on the onset of cell formation in Fe. The tendency for cell formation is retarded as the temperature at which deformation occurs is lowered.

If such a tendency also applies to Nb, a cell structure may not be observed for any deformation at ambient temperature since the deformation temperature is about 2400°C below the melting point.

The current theories[24, 25, 26, 27] of work hardening in metals predict a flow stress that is a linear function of the square root of the dislocation density. These theories are based on cell structure formation or some type of well-defined regions of high dislocation density. It has been shown that a well-defined cell structure is developed with tensile deformation in the specimens giving a tensile curve of type "B". Further, the flow stress for these specimens is a function of the square root of the dislocation density. Hence, a mechanism or mechanisms which are the basis of these theories is thought to apply to these specimens.

The flow stress behavior of the specimens exhibiting tensile curves of type "C" are thought to be indicative of the real work hardening process in Nb. This follows since these specimens were given very high temperature anneals and the substructure prior to tensile deformation was devoid of networks of precipitates. In fact, fairly large areas had to be scanned to observe any dislocations. When dislocations were observed in the substructure they were randomly distributed or associated with small atom clusters and on isolated precipitates.

Current theories of work-hardening do not predict a flow stress that is dependent on $\rho^{\frac{1}{2}}$, therefore correlation of the observed behavior of the flow stress with the theoretical models cannot be made at this time.

6 Summary and Conclusions

1. The lower yield stress of polycrystalline Nb can be expressed by:

$$\tau_{ly} = \tau_f + \tau_{structure} + \tau(\dot{\epsilon}),$$

where τ_f = friction stress = $(\tau_o + \tau_{soln.})$

$\tau_o \doteq 0.8(\frac{kg}{mm^2})$ (lattice friction stress)

$\tau_{soln.} = 0.279 \times 10^3 \times$ (Atom Fraction of Impurities)
(friction stress due to impurities atomistically in solution)

$\tau_{structure} = G\,\epsilon^2\,c$ (stress due to dilations in the crystal from solute atom clusters and precipitates)

G = shear modulus

ϵ = solute atom misfit parameter

$$\epsilon = \frac{(\text{radius solute atom} - \text{radius solvent atom})}{\text{radius solvent atom}}$$

c = Atom Fraction of Impurities

$\tau(\dot{\epsilon})$ = strain rate dependence of the yield strength.

2. The flow stress-plastic strain relation determined from dislocation density measurements correlates with the experimentally observed flow stress-plastic strain relation.

3. The flow stress of polycrystalline Nb is markedly influenced by the initial dislocation substructure. The presence of precipitate networks markedly influences the flow stress, producing a flow stress-dislocation density dependence of:

$$\sigma_{fl}\,(\frac{kg}{cm^2}) = 0.85\,Gb\rho^{\frac{1}{2}} + \text{constant}.$$

The flow stress-dislocation density dependence in fully annealed polycrystalline Nb is given by:

$$\sigma_{fl} \left(\frac{kg}{cm^2}\right) = 6.5 \times 10^3 \, Gb\rho^{\frac{1}{2}} + \text{constant.}$$

4. On the basis of 1, 2 and 3 above, the stress-strain curve of polycrystalline Nb can be predicted beyond the lower yield point when the impurity level, annealing temperature and dislocation density are known.

5. In order to better understand the mechanisms of dislocation interactions in Nb, experiments must be conducted on oriented single crystals where the stress and strain axes can be fixed.

7 Acknowledgements

Greatest appreciation is extended to Professor Thomas and Professor Washburn for their guidance and stimulating discussions which led to the solution of many problems encountered in the research. The guidance and patient teaching of Mr. DeBaar in the use of the electron microscope is also appreciated. The special efforts of Miss Zuck in the thesis typing and the support of the Inorganic Materials Research Division of the Lawrence Radiation Laboratory, under contract to the Atomic Energy Commission, are especially appreciated.

REFERENCES

1. R. Benson, G. Thomas and J. Washburn, "Dislocation Substructures in Deformed and Recovered Molybdenum," Direct Observations of Imperfections in Crystals, Newkirk and Wernick, Eds., Interscience, New York, 1962, p. 375.

2. "Substructure and Mechanical Properties of Refractory Metals," Wright Air Development Division Tech. Report TR-61-19.

3. A. Fourdeux and A. Berghezan, J. Inst. of Metals, 89, 31 (1960).

4. N. J. Petch, J. Iron and Steel Institute, 174, 25, (1959).

5. G. Thomas, Transmission Electron Microscopy of Metals, 154-156, John Wiley and Sons, New York, (1962).

6. R. K. Ham, "The Determination of Dislocation Densities in Thin Films," Phil. Mag., 6, 1183, (1961).

7. J. E. Bailey and P. B. Hirsch, "The Dislocation Distribution, Flow Stress, and Stored Energy in Coldworked Polycrystalline Silver," Phil. Mag., 5, 485 (1960).

8. C. S. Smith and L. Guttman, "Measurement of Internal Boundaries in Three Dimensional Structures by Random Sectioning," J. Metals, New York, 5, 81, (1953).

9. A. H. Cottrell, Dislocations and Plastic Flow in Crystals, 125 Oxford, Clarendon Press, (1953).

10. M. J. Leadbetter and B. B. Argent, "The Effect of Oxygen on the Mechanical Properties of Zone Refined Niobium," J. Less-Common Metals, 3, 1958, (1961).

11. M. B. Reynolds, Trans. A. S. M., 45, 396, (1953).

12. C. S. Barrett, Structure of Metals, 646-648, McGraw-Hill, New York, (1952).

13. W. Hume-Rothery and G. V. Raynor, The Structure of Metals and Alloys, 66, Monograph, Inst. of Metals, London, (1956).

14. G. V. Smith, Properties of Metals at Elevated Temperatures, 55, McGraw-Hill (1950).

15. A. H. Cottrell and B. A. Bilby, Proc. Phys. Soc. A62, 49 (1949)

16. A. S. Keh and S. Weissmann, "Deformation Substructure in Body-Centered C ubic Metals," Electron Microscopy and Strength of Crystals, Thomas and Washburn, Eds., Interscience, (In press).

17. W. G. Johnston, "Yield Points and Delay Times in Single Crystals," Gen. Elec. Res. Laboratory report No. 62-RL-2980M, (1962), to be published in J. App. Phys.

18. A. T. Churchman, J. Inst. Metals, 221 (1960).

19. M. A. Adams, A. C. Roberts and R. E. Smallman, "Yield and Fracture in Polycrystalline Nb," U. K. A. E. A. Rept. H. E. R. E. M/R 2530 (1959).

20. B. A. Wilcox and R. A. Huggins, J. Less-Common Metals, 2, 297 (1960)

21. A. A. Johnson, J. Less-Common Metals, 2, 241 (1960).

22. R. W. Powers and M. V. Doyle, "Some Internal Friction Studies in Columbium, "J. of Metals, New York, 1285 (1957).

23. A. S. Keh and W. C. Leslie, "Recent Observations on Quench-Aging and Strain-Aging of Iron and Steel," North Carolina State College Conference, March 1962, to be published by Interscience Publishers.

24. N. F. Mott, Trans. AIME 218, 962 (1960)

25. G. Saada, (Acta Met. 3, 200 (1960), (Acta Met. 8, 341 (1960) (Acta Met. 9, 166 (1961).

26. A. Seeger, Dislocation and Mechanical Properties of Crystals, 243, John Wiley and Sons, New York (1957).

27. J. C. M. Li, Discussion of paper by Keh, Direct Observations of Imperfections in Crystals, Newkirk, Wernick, Eds., Interscience, New York 1962, p.234.

This report was prepared as an account of Government sponsored work. Neither the United States, nor the Commission, nor any person acting on behalf of the Commission:

A. Makes any warranty or representation, expressed or implied, with respect to the accuracy, completeness, or usefulness of the information contained in this report, or that the use of any information, apparatus, method, or process disclosed in this report may not infringe privately owned rights; or

B. Assumes any liabilities with respect to the use of, or for damages resulting from the use of any information, apparatus, method, or process disclosed in this report.

As used in the above, "person acting on behalf of the Commission" includes any employee or contractor of the Commission, or employee of such contractor, to the extent that such employee or contractor of the Commission, or employee of such contractor prepares, disseminates, or provides access to, any information pursuant to his employment or contract with the Commission, or his employment with such contractor.